

Trinuclear Copper Complexes with Triplesalen Ligands: Geometric and Electronic Effects on Ferromagnetic Coupling via the Spin-Polarization Mechanism

Thorsten Glaser,^{*[a]} Maik Heidemeier,^[a] Julia B. H. Strautmman,^[a] Hartmut Bögge,^[a] Anja Stammler,^[a] Erich Krickemeyer,^[a] Robert Huenerbein,^[b] Stefan Grimme,^[b] Eberhard Bothe,^[c] and Eckhard Bill^[c]

Dedicated to Professor Karl Wieghardt on the occasion of his 65th birthday

Abstract: A series of trinuclear Cu^{II} complexes with the tris(tetradentate) triplesalen ligands H₆talen, H₆talen^{tBu₂}, and H₆talen^{NO₂}, namely [(talen)Cu^{II}₃] (**1**), [(talen^{tBu₂})Cu^{II}₃] (**2**), and [(talen^{NO₂})Cu^{II}₃] (**3**), were synthesized and their molecular and electronic structures determined. These triplesalen ligands provide three salen-like coordination environments bridged in a *meta*-phenylene arrangement by a phloroglucinol backbone. The structure of [(talen)Cu^{II}₃] (**1**) was communicated recently. The structure of the *tert*-butyl derivative [(talen^{tBu₂})Cu^{II}₃] (**2**) was established in three different solvates. The molecular structures of these trinuclear complexes show notable differences, the most important of which is the degree of ligand folding around the central Cu^{II}–phenolate bonds. This folding is symmetric with regard to the central phloroglucinol backbone in two structures, where it gives rise to bowl-shaped overall geometries. For one solvate two trinuclear triplesalen complexes form a supramolecular disk-like arrangement, hosting two dichloromethane molecules like two pearls in an oyster. The FTIR spectra of these com-

plexes indicate the higher effective nuclear charge of Cu^{II} in comparison to the trinuclear Ni^{II} complexes by the lower C–O and higher C=N stretching frequencies. The UV/Vis/NIR spectra of **1–3** reflect the stronger ligand folding in the *tert*-butyl complex **2** by an intense phenolate-to-Cu^{II} LMCT. This absorption is absent in **1** and is obscured by the nitro chromophore in **3**. The more planar molecular structures cause orthogonality of the Cu^{II} d_{x²-y²} orbital and the phenolate O p_z orbital, which leads to small LMCT dipole strengths. Whereas **1** and **3** exhibit only irreversible oxidations, **2** exhibits a reversible one-electron oxidation at +0.26 V, a reversible two-electron oxidation at +0.59 V, and a reversible one-electron oxidation at +0.81 V versus Fc⁺/Fc. The one-electron oxidized form **2**⁺ is strongly stabilized with respect to reference mononuclear salen-like Cu complexes. Chemical one-electron oxidation of **2** to **2**⁺


allows the determination of its UV/Vis/NIR spectrum, which indicates a ligand-centered oxidation that can be assigned to the central phloroglucinol unit by analogy with the trinuclear Ni triplesalen series. Delocalization of this oxidation over three Cu^{II}–phenolate subunits causes the observed energetic stabilization of **2**⁺. Temperature-dependent magnetic susceptibility measurements reveal ferromagnetic couplings for all three trinuclear Cu^{II} triplesalen complexes. The trend of the coupling constants can be rationalized by two opposing effects: 1) electron-withdrawing terminal substituents stabilize the central Cu^{II}–phenolate bond, which results in a stronger coupling, and 2) ligand folding around the central Cu^{II}–phenolate bond opens a bonding pathway between the magnetic Cu^{II} d_{x²-y²} orbital and the phenolate O p_z orbital, which results in a stronger coupling. Density functional calculations indicate that both spin-polarization and spin-delocalization are operative and that slight geometric variations alter their relative magnitudes.

Keywords: copper • magnetic properties • mixed-valent compounds • N,O ligands • spin polarization

[a] Prof. Dr. T. Glaser, Dr. M. Heidemeier, Dipl.-Chem. J. B. H. Strautmman, Dr. H. Bögge, A. Stammler, E. Krickemeyer
Lehrstuhl für Anorganische Chemie I
Universität Bielefeld
Universitätsstrasse 25, 33615 Bielefeld (Germany)
Fax: (+49) 521-106-6003
E-mail: thorsten.glaser@uni-bielefeld.de

[b] Dipl.-Chem. R. Huenerbein, Prof. Dr. S. Grimme
Organisch-Chemisches Institut
Westfälische Wilhelms-Universität
Corrensstrasse 40, 48149 Münster (Germany)

[c] Dr. E. Bothe, Dr. E. Bill
Max-Planck-Institut für Bioanorganische Chemie
Stiftsstrasse 34–36, 45470 Mülheim (Germany)

 Supporting information for this article is available on the WWW under <http://www.chemeurj.org/> or from the author.

Introduction

The current interest in the synthesis of magnetic materials based on molecular entities started with the observation that $[\text{Cp}^*\text{Fe}]^+[\text{TCNE}]^-$ (TCNE = tetracyanoethylene) exhibits a spontaneous long-range ferromagnetic ordering with a Curie temperature, T_C , of 4.8 K.^[1–3] Another milestone in the field of molecule-based magnets was the observation that $[\text{Mn}_{12}\text{O}_{12}(\text{O}_2\text{CCH}_3)_{16}(\text{OH}_2)_4]$ (**Mn₁₂**),^[4] which was the first member of a new class of molecular materials called single-molecule magnets (SMMs),^[5–8] exhibits a hysteresis in its magnetization of pure molecular origin.^[9,10] SMMs possess an energy barrier for spin reversal which causes a slow relaxation of the magnetization at low temperatures. This energy barrier originates from a ground state with large total spin (S_T) and large magnetic anisotropy with an easy axis of magnetization which owes its origin to a negative zero-field splitting parameter D .

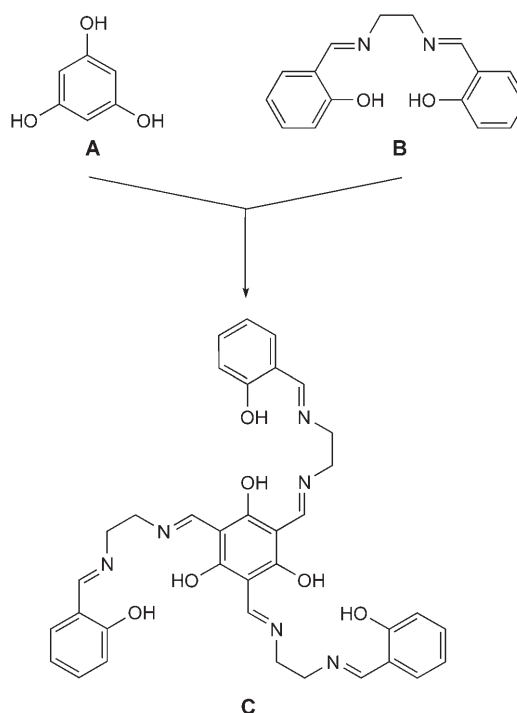
An important research objective in the rational design of new molecule-based magnetic materials, whether long-range ordered magnets or single molecule magnets, is the development of synthetic strategies that lead to molecular building blocks that enforce ferromagnetic interactions and/or high-spin ground states.^[11] We are currently exploring three different strategies to establish synthetic recipes for parallel spin alignments: 1) the double exchange mechanism^[12–14] in face-sharing octahedra,^[15,16] 2) the use of orthogonal magnetic orbitals,^[17–19] and 3) the spin-polarization mechanism^[20,21] in *m*-phenylene-bridged complexes,^[22,23] the latter of which is the subject of the work described herein.

The spin-polarization mechanism is well established in organic chemistry where ferromagnetic interactions are achieved by *m*-phenylene linkages of organic radicals and carbenes.^[24–29] This concept can be applied to transition metal complexes by using various bridging units. Pyrimidine is one of the most frequently used *m*-phenylene bridging unit. Some complexes containing this ligand indeed exhibit ferromagnetic interactions^[30–33] whereas others show antiferromagnetic interactions.^[34–40] The same holds true for the C_3 -symmetric μ_3 -bridging ligand 1,3,5-triazine, which may be regarded as the triangular extension of the μ_2 -bridging ligand pyrimidine, where both ferromagnetically and antiferromagnetically coupled trinuclear Ti^{III} complexes have been reported.^[41,42] Ferromagnetic interactions were also achieved with a modified resorcinol ligand bridging two Fe^{III} centers in a *m*-phenylene arrangement.^[43,44]

In a systematic study,^[45] McCleverty and Ward were able to correlate the exchange coupling in dinuclear Mo complexes of extended polypyridyl^[46] and polyphenol^[47] ligands with the bridging topology by the spin-polarization mechanism. In particular, they observed ferromagnetic interactions in a 1,3-dihydroxy- and a 1,3,5-trihydroxybenzene-bridged Mo^{V} complex, whereas in the 1,4-dihydroxybenzene-bridged complex they observed antiferromagnetic interactions.^[48,49] These authors extended their studies to naphthalene-based dihydroxy systems where the exchange interactions could also be rationalized by the spin-polarization mechanism.^[50]

To synthesize trinuclear phloroglucinol-bridged ligands of the first transition-metal series, we have developed modified 1,3,5-trihydroxybenzene (phloroglucinol) ligands with pendant arms and have shown that the *m*-phenylene arrangement leads to ferromagnetic interactions in trinuclear Cu^{II} complexes.^[22] Closely related ligand systems based on 1,3-di- and 1,3,5-triaminobenzenes that involve mostly ferromagnetic couplings have also been investigated.^[51–56]

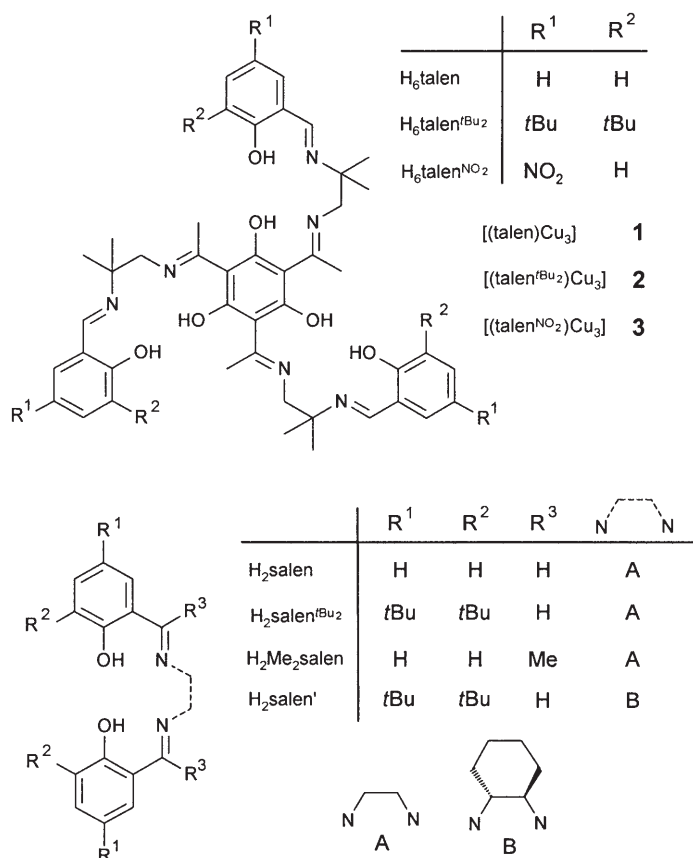
To match the two necessary requirements for SMMs, namely large spin-multiplicity and large negative zero-field splitting with axial symmetry ($E/D=0$), we designed the triplesalen ligand **C** (Scheme 1),^[57] which combines the phloro-



Scheme 1. The hybrid-ligand triplesalen (**C**) comprises a phloroglucinol bridging unit (**A**) for high-spin ground-states by ferromagnetic coupling and a salen-like coordination environment (**B**) for single-site magnetic anisotropy by strong tetragonal ligand-fields.

glucinol bridging unit **A** for ferromagnetic couplings, and thus high-spin ground states, with the coordination environment of a salen ligand **B**, which is known to establish a pronounced magnetic anisotropy due to its strong ligand field in the basal plane.^[58–60] A well-studied example of a similar system is the Jacobsen catalyst $[(\text{salen}')\text{Mn}^{\text{III}}\text{Cl}]$,^[61] which is an Mn^{III} ($S=2$) species with a zero-field splitting, D , of around -2.5 cm^{-1} .^[58,62,63] In this respect, it is interesting to note that dimeric Mn^{III} salen complexes are known to behave as SMMs.^[64]

We have shown that variation of the terminal substituents of the triplesalen ligands in a series of trinuclear nickel complexes (Scheme 2) provides a control of the electronic communication between the metal–salen subunits.^[65] Additional-



Scheme 2. Abbreviations used.

ly, the severe ligand folding observed in $[(\text{talen}^{\text{tBu}_2})\text{Ni}_3]$ results in an overall bowl-shaped molecular structure.

We recently communicated the successful synthesis of the first trinuclear Cu^{II} triplesalen complex $[(\text{talen})\text{Cu}_3]$, which exhibits an $S_1=3/2$ spin ground state.^[23] The EPR spectrum of this complex displays a ten-line hyperfine splitting pattern due to the coupling of the total electron spin with the individual Cu nuclear spins ($I=3/2$) according to the $2 \times n \times I + 1$ rule. Density functional calculations demonstrated that the spin-density on adjacent carbon atoms of the central benzene rings alters in the quartet ground state, in accordance with the spin-polarization mechanism.^[23]

We have taken advantage of the ligand folding in triplesalen complexes by treating two equivalents of a trinuclear Mn^{III} triplesalen complex with $[\text{Cr}(\text{CN})_6]^{3-}$. The ligand folding in the *tert*-butyl derivative preorganizes the three Mn^{III} ions for coordination of three facial nitrogen atoms of $[\text{Cr}(\text{CN})_6]^{3-}$. The resulting complex, $[\{(\text{talen}^{\text{tBu}_2})\text{Mn}^{\text{III}}\}_2\text{Cr}^{\text{III}}(\text{CN})_6\}](\text{BPh}_4)_3 \cdot 4\text{CH}_3\text{CN} \cdot 2\text{Et}_2\text{O}$ (**Mn₆Cr**-(BPh₄)₃·4CH₃CN·2Et₂O), fulfils all the requirements for a single-molecule magnet. AC susceptibility and hysteresis measurements proved that this complex is a single-molecule magnet with a high anisotropy barrier.^[66] However, when simulating the temperature-dependence of the magnetic properties of the **Mn₆Cr**³⁺ ion, we found that the coupling between the Mn^{III} ions in this trinuclear Mn^{III} triplesalen

building block is slightly antiferromagnetic and not, as expected, ferromagnetic. This behaviour was also found in the nitro-substituted trinuclear Mn^{III} triplesalen complex $[(\text{talen}^{\text{NO}_2})\{\text{Mn}^{\text{III}}(\text{DMSO})_2\}_3](\text{ClO}_4)_3$.^[67]

To better understand the spin-polarization mechanism in transition-metal chemistry in general, and in phloroglucinol-bridged complexes in particular, we herein present a study of trinuclear Cu^{II} triplesalen complexes. The ligand folding in these complexes is strongly dependent on the nature of the terminal substituent and on the crystallization solvent. This study allows the influence of the ligand folding, and therefore of the orientation of the magnetic orbitals, on the spin-polarization properties to be determined. Correlation of the structural and magnetic properties leads to important insights into the spin-polarization mechanism and its application to obtaining ferromagnetic interactions in transition-metal complexes.

Besides our interest in the magnetic properties, variation of the ligand folding in the triplesalen complexes should allow systematic investigations of enantioselective transformations. While metal salen complexes have been known for a long time to catalyze chemical transformations,^[68–76] the discovery by Jacobsen, Katsuki, and co-workers that chiral Mn^{III} salen complexes are effective catalysts for the enantioselective epoxidation of unfunctionalized olefins^[61,77–80] led to a revival in the chemistry of salen ligands. A folded geometry of the salen ligand accompanied by the formation of a chiral pocket has been argued to be an essential element for their enantioselectivity.^[81–89] Additionally, a cooperative reactivity between multiple metal centers in covalently linked salen systems has been established,^[90,91] therefore trinuclear triplesalen complexes might have useful applications in enantioselective catalysis.

Experimental Section

Preparation of compounds: H₆talen [2,4,6-tris(1-(2-salicylaldimino-2-methylpropylimino)ethyl)-1,3,5-trihydroxybenzene], H₆talen^{tBu₂} [2,4,6-tris(1-(2-(3,5-di-*tert*-butylsalicylaldimino)-2-methylpropylimino)ethyl)-1,3,5-trihydroxybenzene], H₆talen^{NO₂} [2,4,6-tris(1-(2-(5-nitrosalicylaldimino)-2-methylpropylimino)ethyl)-1,3,5-trihydroxybenzene], and $[(\text{talen})\text{Cu}_3]$ (**1**) were synthesized as described previously.^[23,57,65]

$[(\text{talen}^{\text{tBu}_2})\text{Cu}_3]$ (2**):** A solution of Cu(OAc)₂·H₂O (55 mg, 0.27 mmol) in EtOH (10 mL) was added dropwise to a suspension of H₆talen^{tBu₂} (100 mg, 90 μmol) in EtOH (10 mL) and the resulting brown solution was heated to reflux for 30 min. The purple fibrous precipitate that formed upon cooling to room temperature was filtered off, washed with Et₂O, and dried under vacuum. Yield: 87 mg (75%). MALDI-TOF MS: m/z 1295.5 [M]⁺; IR (KBr): $\tilde{\nu}$ = 2960m, 2905w, 2868w, 1623s, 1560s, 1546s, 1530m, 1476vs, 1431s, 1390m, 1363w, 1337w, 1289m, 1256w, 1192w, 1166w, 840w, 541w cm⁻¹; elemental analysis calcd (%) for C₆₉H₉₆Cu₃N₆O₆·H₂O (1314.2): C 63.06, H 7.52, N 6.39; found: C 63.19, H 7.30, N 6.12.

$[(\text{talen}^{\text{NO}_2})\text{Cu}_3]$ (3**):** A solution of H₆talen^{NO₂} (200 mg, 0.22 mmol) in DMF (3 mL) was added dropwise to a solution of Cu(OAc)₂·H₂O (134 mg, 0.67 mmol) in DMF (3 mL) and the resulting brown solution was stirred at 70°C for 2 h. The purple fibrous precipitate that formed upon cooling to room temperature was filtered off, washed with Et₂O, and dried under vacuum. Yield: 156 mg (65%). MALDI-TOF MS: m/z 1094.5 [M]⁺; IR (KBr): $\tilde{\nu}$ = 3063w, 2967w, 2929w, 1642m, 1606m, 1556s,

1462s, 1390m, 1324vs, 1286m, 1244w, 1193w, 1102m, 949w, 844w, 682w cm⁻¹; elemental analysis calcd (%) for C₄₅H₄₅Cu₃N₆O₁₂·H₂O (1112.6): C 48.58, H 4.26, N 11.33; found: C 48.78, H 4.04, N 11.34.

Oxidation of 2 to 2⁺ with one equivalent of [(C₆H₄Br)₃N](SbCl₆) (AR):

This reaction was carried out using two Schlenk flasks cooled in a cryostat. A dip probe connected to a UV/Vis spectrometer was placed in one of the Schlenk flasks. Dry CH₂Cl₂ (40 mL in the Schlenk flask equipped with the dip probe and 5 mL in the other Schlenk flask) was cooled to -30°C under argon and the background spectrum of CH₂Cl₂ was taken. The solvent was then warmed to room temperature and AR (6.12 mg, 7.50 μmol) was transferred into the Schlenk flask without the dip probe. CH₂Cl₂ (20 mL) was taken out of the Schlenk flask equipped with the dip probe and added to the Schlenk flask containing AR. A portion of 2·0.7 C₆H₁₄ (8.14 mg, 6.00 μmol) was then added to the flask with the dip probe. Both solutions were stirred for 1 h and then cooled to -30°C. The solution of AR (20 mL, 6.00 μmol) was added quickly to the solution of 1 by syringe transfer and the UV/Vis spectrum was recorded.

X-ray crystallography: Crystals of 2a–2e were removed from their respective mother liquors and immediately cooled to the temperature given in Table 1. Data for compounds 2a and 2c–2e were recorded with a Bruker AXS SMART diffractometer (three-circle goniometer with a 1 K CCD detector, Mo_{Kα} radiation, graphite monochromator; sphere of data collected for 2a and 2c, hemisphere of data collected for 2d and 2e with ω-scans with a 0.3° scan width and a detector distance of 5 cm). A hemisphere of data for compound 2b was measured with a Bruker AXS APEX diffractometer equipped with a rotating anode with ω- and φ-scans with a 0.3° scan width. Empirical absorption corrections using equivalent reflections were performed with the program SADABS. The structures were solved with the program SHELXS-97 and refined using SHELXL-97 (SHELXS/L, SADABS from G. M. Sheldrick, University of Göttingen, Germany 1997/2001). Crystal data and further details concerning the crystal structure determination are summarized in Table 1. CCDC-638570 (2b), CCDC-638571 (2a), CCDC-638572 (2d), CCDC-

638573 (2c), and CCDC-638574 (2e) contain the supplementary crystallographic data for this paper. These data can be obtained free of charge from the Cambridge Crystallographic Data Centre via www.ccdc.cam.ac.uk/data_request/cif.

Magnetic measurements: The single crystals lose solvent when they are extracted from their respective mother liquors and especially during the purge-and-thaw cycles in the magnetometer. We used the following procedure to determine the exact composition and identity of the samples used for the magnetic measurements. First of all we measured the FTIR spectra and performed elemental analysis on the single crystals. As low pressures are applied to the sample in the magnetometer, and as we needed to be sure that no further solvent loss occurs during the measurements, we then stored the ground microcrystals over a period of 24 h under a dynamic vacuum of 0.005 mbar. After this vacuum treatment, we measured the weight loss and FTIR spectra and performed a new elemental analysis. Comparison of the FTIR spectra, which are sensitive to the molecular structure, before and after the vacuum treatment established that the trinuclear complexes do not change during the purge-and-thaw cycles. The linewidths of the FTIR spectra do not change after this vacuum treatment, thereby indicating no significant change in the homogeneity of the sample. This suggests, but does not prove, that the ligand folding does not change significantly due to solvent loss. The compositions of the samples were evaluated by weight loss and elemental analyses. Temperature-dependent magnetic susceptibilities were measured with a SQUID magnetometer (Quantum Design) at 1.0 T (2.0–300 K). For calculations of the molar magnetic susceptibility, χ_M, the measured susceptibilities were corrected for the underlying diamagnetism of the sample holder and the sample by using tabulated Pascal's constants. The JulX program package was used for spin-Hamiltonian simulations and fitting of the data by a full-matrix diagonalization approach.^[92]

Other physical measurements: Infrared spectra (400–4000 cm⁻¹) of solid samples were recorded with a Bruker Vector 22 spectrometer as KBr disks. UV/Vis/NIR absorption spectra of solutions were recorded with a

Table 1. Crystallographic data for 2a, 2b, 2c, 2d, and 2e.

Compound	2a	2b	2c	2d	2e
empirical formula	C ₆₉ H ₉₆ Cu ₃ N ₆ O ₆ ·(C ₆ H ₁₆) _{0.8} (CH ₂ Cl ₂) _{0.2}	C ₆₉ H ₉₆ Cu ₃ N ₆ O ₆ ·2.5 CH ₂ Cl ₂	C ₆₉ H ₉₆ Cu ₃ N ₆ O ₆ ·(C ₆ H ₁₄) _{0.7} (CH ₂ Cl ₂) _{0.3}	C ₆₉ H ₉₆ Cu ₃ N ₆ O ₆ ·2.5 CH ₂ Cl ₂	C ₆₉ H ₉₆ Cu ₃ N ₆ O ₆ ·3.5 CHCl ₃
formula weight	1397.51	1508.45	1381.94	1508.45	1713.93
T [K]	183(2)	173(2)	183(2)	173(2)	183(2)
crystal system	triclinic	monoclinic	triclinic	monoclinic	rhombohedral
space group	P $\bar{1}$	C2/c	P $\bar{1}$	C2/c	R $\bar{3}c$
a [Å]	14.1180(6)	32.7135(16)	14.1051(6)	32.7631(17)	19.1400(9)
b [Å]	16.9442(7)	22.4939(11)	16.9098(7)	22.5388(11)	
c [Å]	17.2839(7)	23.1956(12)	17.3196(7)	23.1968(12)	79.887(5)
α [°]	69.834(1)		69.860(1)		
β [°]	81.045(1)	113.517(1)	81.078(1)	113.375(1)	
γ [°]	81.046(1)		80.984(1)		
V [Å ³]	3810.6(3)	15650.9(14)	3807.6(3)	15723.6(14)	25 345(2)
Z	2	8	2	8	12
ρ _{calcd} [Mg m ⁻³]	1.218	1.280	1.205	1.274	1.348
μ [mm ⁻¹]	0.895	1.029	0.902	1.024	1.130
crystal color/shape	red-purple/needles	red-purple/columns	red-purple/needles	red-purple/columns	brown/hexagonal plates
crystal size [mm]	0.40 × 0.05 × 0.02	0.12 × 0.05 × 0.01	0.50 × 0.04 × 0.01	0.50 × 0.10 × 0.04	0.30 × 0.30 × 0.03
θ range [°]	1.48–27.02	1.30–25.00	1.48–27.02	1.29–27.00	1.53–25.00
reflections collected	39 681	62 755	39 302	61 127	41 280
unique reflections	16 380	13 793	16 350	17 070	4964
reflections	(R(int) = 0.0471)	(R(int) = 0.0979)	(R(int) = 0.0373)	(R(int) = 0.0471)	(R(int) = 0.0648)
observed reflections (I > 2σ(I))	10 256	9 313	10 892	12 332	3681
max./min. transmission	0.9823/0.7160	0.9898/0.8865	0.9910/0.6612	0.9602/0.6285	0.9669/0.7280
data/restraints/parameters	16 380/27/813	13 793/17/882	16 350/20/821	17 070/10/859	4964/3/315
goodness-of-fit on F ²	1.013	1.036	1.020	1.067	1.204
final R indices (I > 2σ(I))	R1 ^[a] = 0.0476, wR2 ^[a] = 0.1129	R1 = 0.0610, wR2 = 0.1296	R1 = 0.0483, wR2 = 0.1095	R1 = 0.0536, wR2 = 0.1285	R1 = 0.0847, wR2 = 0.2004
largest diff. peak/hole [e Å ⁻³]	0.500/−0.416	0.512/−0.735	0.667/−0.455	0.774/−0.791	0.742/−0.570

[a] R1 = Σ||F_o − |F_c||/Σ|F_o|; wR2 = [Σw(F_o² − F_c²)²/Σw(F_o²)²]^{1/2}.

Varian Cary 50 spectrophotometer in the range 190–1100 nm at ambient temperature. The UV/Vis absorption spectrum of oxidized **2⁺** was recorded with a custom-made Hellma 661.087-UVS dip probe connected to a J&M TIDAS II diode-array UV/Vis spectrometer via fibre-glass optics. The Schlenk flasks were cooled in-line with a Julabo F81-ME circulation cryostat. MALDI-TOF mass spectra were recorded with a Bruker Reflex IV mass spectrometer (matrix: DCTB). The electrochemical experiments were performed with argon-flushed CH₂Cl₂ solutions containing 0.2 M [NBu₄]⁺PF₆⁻ in a classical three-electrode cell. The working electrode was a glassy carbon disk electrode, the counter electrode a platinum wire, and the reference electrode was Ag/0.01 M AgNO₃/CH₃CN. All potentials are referenced to the ferrocenium/ferrocene (Fc⁺/Fc) couple as internal standard. The electrochemical cell was connected to an EG&G potentiostat/galvanostat (model 273 A).

Computational details: Theoretical calculations were carried out using the TURBOMOLE 5.7 suite of programs.^[93] The computations on the model system were performed at the unrestricted density functional theory (U-DFT) level employing the B-P86 functional^[94,95] and the resolution of identity (RI) approximation^[96,97] for the two-electron integrals. A Gaussian AO basis set of triple- ξ quality with polarization functions on all atoms (TZVP)^[98] and a numerical quadrature multiple grid (“grid m4” in TURBOMOLE nomenclature) were used. The atomic spin densities were obtained by a Mulliken population analysis. The $\langle S^2 \rangle$ values for all computed quartet states were close to the expected value for a pure quartet (3.75).

Results

Synthesis and characterization: Following the reaction procedure for the synthesis of [(talⁿ)Cu₃] (**1**),^[23] the reaction of H₆tal^{nBu₂} with copper acetate in EtOH afforded [(tal^{nBu₂})Cu₃] (**2**) as a purple, microcrystalline solid. The preparation of purple microcrystalline [(tal^{nO₂})Cu₃] (**3**) was performed in DMF due to the poor solubility of H₆tal^{nO₂} in alcoholic solvents. The successful synthesis of the trinuclear copper complexes was confirmed by MALDI-TOF mass spectrometry and elemental analysis. Both **1** and **2** are soluble in aprotic organic solvents such as CH₂Cl₂, CHCl₃, CH₃CN, or toluene, similar to the corresponding nickel complexes, whereas **3** is only sparingly soluble in DMF and to an ever lesser extent in CH₂Cl₂.

The FTIR spectrum of **2** is almost identical to that of [(tal^{nBu₂})Ni₃]. Two prominent exceptions are the bands at 1623 and 1289 cm⁻¹ in the spectrum of **2**, which appear at 1615 and 1300 cm⁻¹, respectively, in the spectrum of the corresponding Ni complex. These shifts corroborate the assignment of the band at 1623 cm⁻¹ to the C=N aldimine stretch and the band at 1289 cm⁻¹ to the C–O stretch. The C=N ketimine stretch mixes with the C–C stretch of the central phloroglucinol, which leads to only small variations upon changing the metal ion.^[65]

The FTIR spectrum of **3** is almost superimposable on the spectrum of [(tal^{nO₂})Ni₃], with a shift of the C–O band from 1299 cm⁻¹ in the Ni complex^[65] to 1286 cm⁻¹ in **3**. In contrast to [(tal^{nBu₂})Ni₃], two bands are observed at 1606 and 1623 cm⁻¹ in [(tal^{nO₂})Ni₃].^[65] Similarly, a well separated band at 1642 cm⁻¹ is observed in **3**, thereby suggesting the assignment to the C=N aldimine stretch.

The differences in the IR spectra reflect the higher effective nuclear charge of Cu^{II} compared to Ni^{II}. This higher ef-

fective nuclear charge forces the phenolate oxygen to donate more charge to Cu^{II}, which results in less π -bonding of the phenolate oxygen to the aromatic ring and, thus, a lower C–O stretching frequency. On the other hand, the higher effective nuclear charge of Cu^{II} also reduces its π -backbonding to the C=N π orbitals of the imines, therefore the C=N double bond stretching frequency is higher in the Cu complexes.

Structural characterization: No crystals of **3** suitable for a single-crystal X-ray diffraction study were obtained due to its poor solubility. Complex **2**, on the other hand, could be crystallized from different solvent mixtures to yield a variety of crystal forms with different crystal structures and some variation in the ligand folding in the associated molecular structures. This variation in the ligand folding enables a direct correlation of the exchange coupling between the Cu^{II} ions with the folding angle, therefore these crystal structures will be discussed in detail.

Slow evaporation of *n*-heptane/CH₂Cl₂ solutions of **2** yielded crystals with two different morphologies, namely very thin, red-purple needles (**2a**) as the major component and thin, red-purple columns (**2b**) as a very minor component. Slow evaporation of *n*-hexane/CH₂Cl₂ solutions of **2** also yielded crystals with two different morphologies where the major component is again comprised of thin, red-purple needles (**2c**) and the minor component thin, red-purple columns (**2d**). Slow evaporation of *n*-heptane into a CHCl₃ solution of **2** yielded thin, dark-brown hexagonal plates (**2e**). The crystal structures of **2a–2e** were determined by single-crystal X-ray diffraction studies.

Both **2a** and **2c** crystallize in the space group *P* $\bar{1}$ with nearly identical cell constants. It turned out that the crystal structures of **2a** and **2c** are isostructural. Both contain one position for a nonbonded solvent molecule, the nature of which apparently does not influence the crystal structure. This position is occupied statistically in **2a** by CH₂Cl₂ or heptane, while it is occupied statistically in **2c** by CH₂Cl₂ or hexane. The refinement results in the formulation of **2a** as 2·0.8 C₇H₁₆·0.2 CH₂Cl₂ and **2c** as 2·0.7 C₆H₁₄·0.3 CH₂Cl₂. The different occupations of the solvent positions have no significant influence on the molecular structure of **2** in **2a** and **2c**, therefore only the molecular structure of **2c** will be discussed below.

Both **2b** and **2d** crystallize in the space group *C*2/*c* and appear to be identical (2·2.5 CH₂Cl₂), therefore only the molecular structure of **2d** will be discussed below. Solvate **2e** crystallizes in the space group *R* $\bar{3}c$ and refines as 2·3.5 CHCl₃.

The molecular structure of **2** in crystals of **2c** is displayed in Figure 1. In all the structures of **2** the deprotonated triplesalen ligand (tal^{nBu₂})⁶⁻ as well as (talⁿ)⁶⁻ in **1** coordinate three Cu^{II} ions. The Cu^{II} ions are four-coordinate in a square-planar coordination environment of two phenolate and two imine donor atoms. Selected interatomic distances for **2** in crystals of **2c**, **2d**, and **2e**, and for **1** in crystals of 1·CHCl₃·0.5 C₇H₈,^[23] are summarized in Table 2 for comparison.

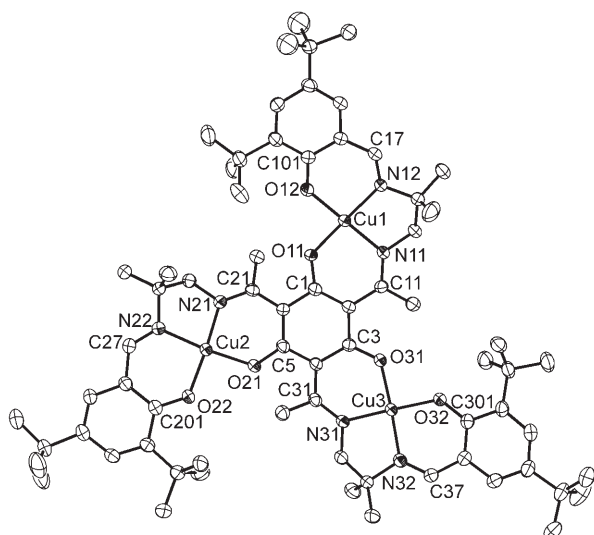


Figure 1. Representative molecular structure of the trinuclear Cu triplesalen complex **2** in crystals of **2c** along with the labeling scheme used. Thermal ellipsoids are drawn at the 50% probability level and hydrogen atoms have been omitted for clarity.

Table 2. Selected interatomic distances [Å] for the trinuclear copper triplesalen complexes.

	1 ^[23]	2c	2d	2e
Cu1–O11	1.883(3)	1.866(2)	1.881(3)	1.892(5)
Cu1–O12	1.899(3)	1.886(3)	1.890(3)	1.890(5)
Cu1–N11	1.942(3)	1.928(3)	1.927(3)	1.945(6)
Cu1–N12	1.940(3)	1.924(3)	1.939(3)	1.935(6)
Cu2–O21	1.859(3)	1.912(2)	1.894(3)	
Cu2–O22	1.899(3)	1.915(3)	1.895(3)	
Cu2–N21	1.930(3)	1.937(3)	1.927(3)	
Cu2–N22	1.923(3)	1.953(3)	1.937(3)	
Cu3–O31	1.883(3)	1.894(3)	1.883(3)	
Cu3–O32	1.916(3)	1.923(3)	1.901(3)	
Cu3–N31	1.921(3)	1.937(3)	1.928(3)	
Cu3–N32	1.935(3)	1.935(3)	1.934(3)	
Cu1...Cu2	7.078(1)	7.115(1)	6.941(1)	6.703(2)
Cu2...Cu3	7.229(1)	7.314(1)	7.113(1)	
Cu3...Cu1	7.211(1)	7.280(1)	7.071(1)	

An important difference in the molecular structures is the overall geometry, which is influenced by the ligand folding. In the series of trinuclear nickel complexes, an almost flat structure is observed for the nitro-substituted [(talen^{NO₂})Ni₃] and a bowl-shaped structure for the *tert*-butyl derivative [(talen^{tBu₂})Ni₃]; no systematic ligand folding is observed for the unsubstituted complex [(talen)Ni₃].^[65] A similar, although not identical, behavior is observed for the trinuclear copper complexes. Figure 2 shows a view of the trinuclear complexes in **1**-CHCl₃·0.5C₇H₈, **2c**, **2d**, and **2e**. A qualitative comparison shows some ligand folding in **1** although it is not regular. Ligand folding is observed at one Cu center in **2c**, while the other two Cu centers exhibit only a small degree of ligand folding. The severe and regular ligand folding observed in **2d** gives rise to the formation of a bowl-shaped structure, and this ligand folding is even more pronounced in **2e**. We have used several parameters to obtain a quanti-

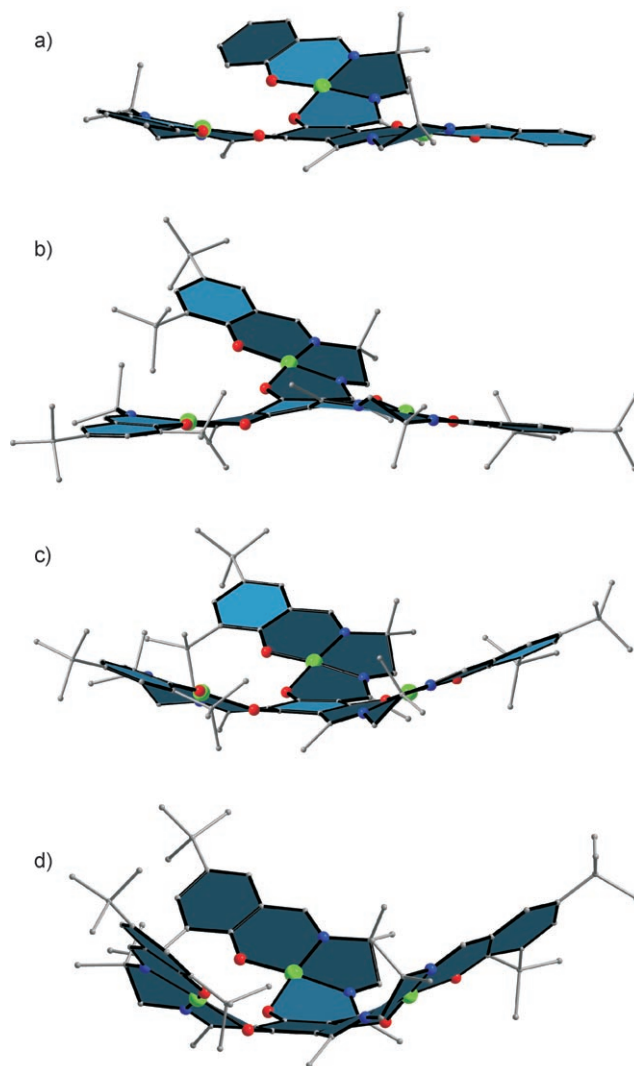


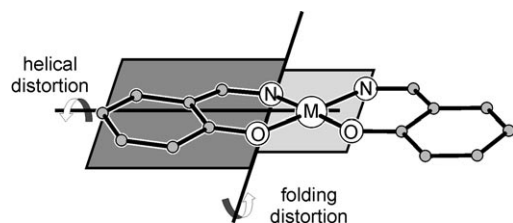
Figure 2. Molecular structures of **1** in crystals of **1**-CHCl₃·0.5C₇H₈ (a)^[23] and **2** in crystals of **2c** (b), **2d** (c), and **2e** (d) drawn perpendicular to the central phloroglucinol ring to emphasize the various degrees of ligand folding. Color code: Cu green, O red, N blue, C gray.

tative description of the ligand folding in our study of the trinuclear nickel triplesalen complexes.^[65] The values of these parameters are summarized for the trinuclear copper triplesalen complexes in Table 3. While all these parameters quantitatively confirm the visual estimate of the ligand folding, we will only focus on the angles ϕ_{central} and ϕ_{terminal} as these are best suited for differentiating between a bending along an idealized line through neighboring N and O ligands and a line perpendicular to the former resulting in a helical distortion (Scheme 3).^[65,88] A close inspection of the calculated values demonstrates that the folding of the terminal phenolates is relatively small compared to the folding of the central phenolates. The angle ϕ_{central} reflects the small ligand folding in **1** and the strong ligand folding in **2e**. The angles for **2c** and **2d** (19.7° and 19.8°, respectively) both indicate a relatively strong ligand folding. However, while this ligand folding is relatively uniform in **2d**, giving an overall bowl-

Table 3. Selected structural properties for the copper triplesalen complexes **1** and **2** in the solvates given.

		1 ·CHCl ₃ ·0.5 C ₇ H ₈	2c	2d	2e
$d^{[a]}$ [Å]	Cu1	0.96	0.97	0.96	1.24
	Cu2	0.65	0.25	0.91	
	Cu3	0.13	-0.46	0.66	
	Mean	0.58	0.56	0.84	1.24
$\alpha^{[b]}$ [°]	Cu1	25.5	28.5	27.9	36.8
	Cu2	15.9	13.9	24.1	
	Cu3	7.3	20.2	18.9	
	mean	16.2	20.9	23.6	36.8
$\beta^{[c]}$ [°]	Cu1	8.8	1.4	3.9	8.5
	Cu2	6.3	9.9	10.9	
	Cu3	11.6	11.0	6.5	
	mean	8.9	7.4	7.1	8.5
$\gamma^{[d]}$ [°]	Cu1	25.4	29.7	29.8	41.2
	Cu2	17.8	7.1	22.3	
	Cu3	18.9	16.5	23.4	
	mean	20.7	17.8	25.2	41.2
$\phi^{\text{central}[e]}$ [°]	Cu1	17.0	20.7	24.4	30.2
	Cu2	7.5	16.4	18.4	
	Cu3	12.1	22.0	16.7	
	mean	12.2	19.7	19.8	30.2
$\phi^{\text{terminal}[e]}$ [°]	Cu1	2.0	6.8	7.5	8.6
	Cu2	1.2	8.3	2.9	
	Cu3	3.1	10.4	8.5	
	mean	2.1	8.5	6.3	6.3

[a] d is the shortest distance between a copper ion and the best plane formed by the six carbon atoms of the central benzene of the phloroglucinol backbone. [b] α is the angle between the best planes of the N₂O₂ and benzene moieties of the central phloroglucinol backbone. [c] β is the angle between the best planes of the N₂O₂ and benzene moieties of the terminal phenolate. [d] γ is the angle between the best planes of the benzene moiety of the central phloroglucinol backbone and the benzene moiety of the terminal phenolate. [e] The bending angle $\phi = 180^\circ - \angle(\text{M}-\text{X}_{\text{NO}}-\text{X}_{\text{R}})$, where X_{NO} is the midpoint between adjacent N and O donor atoms and X_R is the midpoint of the six-membered chelate ring containing these N and O donor atoms.



Scheme 3.

shaped molecular structure, the ligand folding of **2c** is not uniform. Especially the folding of the salen subunit of Cu₃ to the other sites of the phloroglucinol backbone as compared to Cu₁ and Cu₂ prohibits the formation of a bowl-shaped structure.

One unexpected feature is the formation of a supramolecular arrangement in **2d** where two bowl-shaped trinuclear complexes **2** form a disc-like arrangement that hosts two CH₂Cl₂ molecules like two pearls in an oyster (Figure 3). Interestingly, these two trinuclear complexes do not form a staggered conformation but the relative orientation is somewhere between an eclipsed and a staggered conformation (Figure 3a). A close inspection of the intermolecular contacts in combination with the observed nonstaggered confor-

mation indicates that there are some attractive supramolecular interactions between the *tert*-butyl phenol groups that enforce the overall disc-like aggregate. The space between these groups is filled with solvent molecules. We have found a similar supramolecular arrangement in a trinuclear iron triplesalen complex.^[99]

Electrochemistry: We recorded the cyclic (CVs) and square-wave voltammograms (SWs) of **1–3** in CH₂Cl₂ solution. All potentials are referenced to the Fc⁺/Fc couple.

The unsubstituted complex **1** (Figure 4) exhibits one reversible reduction wave at $E_{1/2} = -1.84$ V, which can be attributed to the Cu^{II}/Cu^I couple.^[100] Three irreversible oxidations are observed with peak potentials at $E_p = +0.61$, $+0.77$, and $+0.91$ V. The irreversibility of these oxidations is in accordance with the electrooxidative polymerization observed in unsubstituted copper salen complexes.^[101]

The *tert*-butyl substituted complex **2** exhibits three reversible oxidation waves at $E^1_{1/2} = +0.26$, $E^2_{1/2} = +0.59$, and $E^3_{1/2} = +0.81$ V at -30°C (Figure 5a,b). The peak current of the oxidation E^2 is about twice that of E^1 and is also markedly higher than that of E^3 . Since E^1 is a one-electron oxidation (see below), we assume that E^2 is a two-electron oxidation and E^1 and E^3 correspond to one-electron oxidations. Attempts to split the two-electron oxidation into two separate one-electron oxidations by using fast scan-rates (up to 6 V s^{-1} at a micro electrode) failed. The oxidation E^1 remains reversible upon either warming the solution from -30°C to room temperature or decreasing the scan rate (CV) or frequency (SW), although a fourth oxidation wave with a SW peak at $E^4 = 0.71$ V grows in (Figure 5c) with a concomitant decrease of E^2 and E^3 . This behavior is reversible.

The oxidized trinuclear complex **2⁺** was generated chemically at -40°C by adding one equivalent of the aminyl radical [(C₆H₄Br)₃N][SbCl₆] to a solution of **2** in dichloromethane.

The nitro-substituted complex **3** exhibits only one irreversible oxidation wave with a CV peak potential at $E_p = 0.45$ V (Figure 6).

Electronic absorption spectroscopy: The electronic absorption spectra of complexes **1–3** are characterized by very intense transitions above 23000 cm^{-1} (Figure 7; the spectrum of the mononuclear model compound [(salen)Cu] is included for comparison). The absorption spectrum of [(salen)Cu] consists of a weak band at 17600 cm^{-1} ($300\text{ M}^{-1}\text{ cm}^{-1}$), a band at 27700 cm^{-1} ($10 \times 10^3\text{ M}^{-1}\text{ cm}^{-1}$) with a shoulder at 26300 cm^{-1} , and more intense bands above 32000 cm^{-1} . The low energy band at 17600 cm^{-1} can be assigned to d–d transitions^[102–104] and the transitions above 32000 cm^{-1} to ligand $\pi \rightarrow \pi^*$ transitions. It is interesting to note that several assignments have been reported for the absorptions in the $25000\text{–}30000\text{ cm}^{-1}$ range, including Cu^{II}→phenolate MLCT, phenolate→Cu^{II} LMCT, Cu^{II}→imine MLCT, and intraligand transitions.^[105–108] Whilst not attempting to provide a detailed assignment, the absence of similar strong absorptions in the spectra of the free ligand H₂salen and its deprotonated anionic form salen²⁻ indicates at least some copper

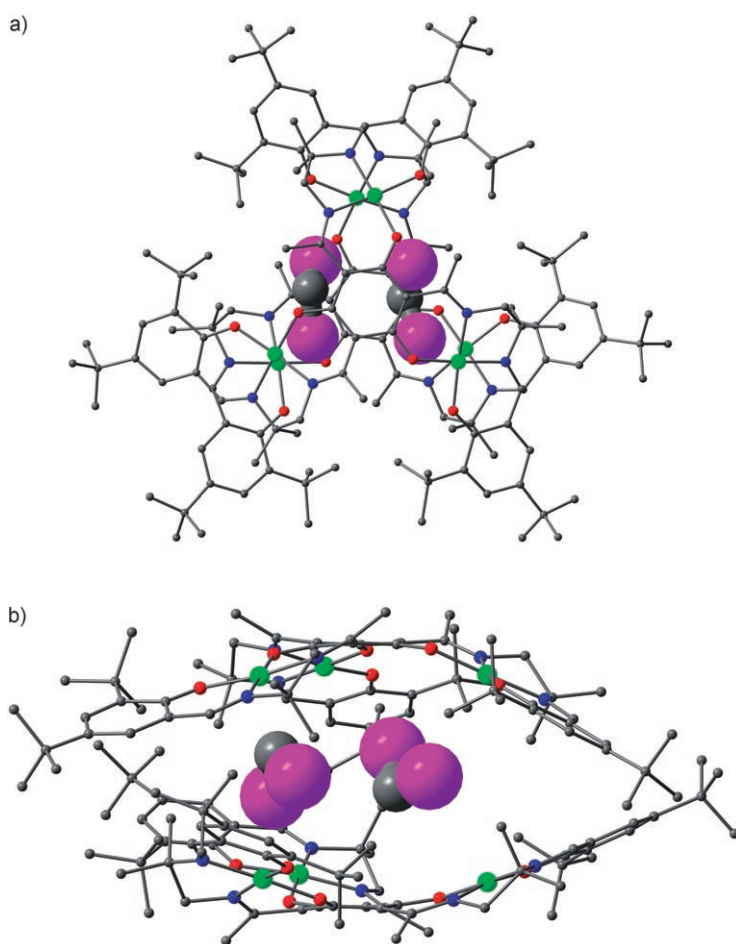


Figure 3. The supramolecular arrangement of two triplesalen complexes **2** and two CH_2Cl_2 molecules in crystals of **2d** is like two pearls in an oyster. Color code: Cu green, O red, N blue, C gray, Cl violet.

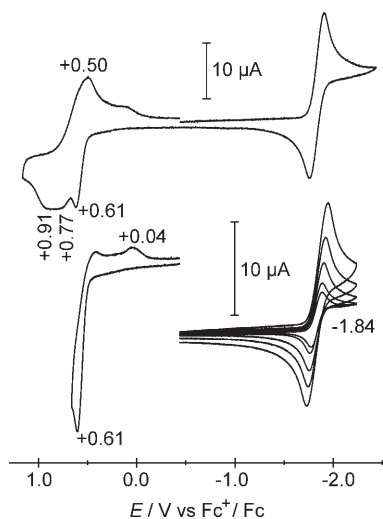


Figure 4. Cyclic voltammograms of **1** in CH_2Cl_2 at 20°C recorded at a glassy carbon working electrode. Scan rate: 200 mVs^{-1} or varying scan rates of 50, 100, 200, 400, and 800 mVs^{-1} .

character for these transitions. The strongly decreased intensity of the absorption corresponding to the reduced tetrahy-

dro salen (“salan”) ligand in its Cu^{II} complex^[105,109,110] further indicates significant amounts of $\text{Cu}^{\text{II}} \rightarrow \text{imine}$ MLCT and imine $\pi \rightarrow \pi^*$ character in these transitions in $[(\text{salen})\text{Cu}]$. We have recently studied an extended system based on 1,8-naphthalenediol where TD-DFT calculations reveal that the orbitals involved in these transitions are strongly delocalized over the whole ligand, with only small contributions from the Cu^{II} ions.^[111]

The electronic absorption spectrum of the trinuclear Cu^{II} complex **1** is remarkably similar to that of $[(\text{salen})\text{Cu}]$ although the intensity increases by roughly a factor of 2, which corresponds to the ratio of four phenol units in **1** compared to two phenol units in $[(\text{salen})\text{Cu}]$. The d–d transitions appear at 17700 cm^{-1} ($780\text{ M}^{-1}\text{cm}^{-1}$) and the CT transitions at 27300 cm^{-1} ($21 \times 10^3\text{ M}^{-1}\text{cm}^{-1}$), with a shoulder at 26100 cm^{-1} .

The absorption spectrum of **2** is similar to that of **1** although there is a new strong band at 30200 cm^{-1} ($60 \times 10^3\text{ M}^{-1}\text{cm}^{-1}$) in the spectrum of **2** which is absent from the spectra of **1**, $[(\text{salen})\text{Cu}^{\text{II}}]$, and the mononuclear *tert*-butyl analogue $[(\text{salen}')\text{Cu}]$.^[110] This is in contrast to the corresponding nickel triplesalen complexes where only the extinction coefficients change on going from $[(\text{talen})\text{Ni}_3]$ to $[(\text{talen}^{\text{tBu}_2})\text{Ni}_3]$.^[65] We cannot give a definitive assignment for the intense band at 30200 cm^{-1} in **2**, although it is interesting to speculate that this strong band may be related to the differences in the ligand folding. While the degree of ligand folding in the trinuclear copper triplesalen complexes in solution is not known, it can be concluded from the solid-state structural analysis that there is a more pronounced ligand folding in **2** than in **1**. This ligand bending produces an additional phenolate $p_z \rightarrow \text{Cu}^{\text{II}} d_{x^2-y^2}$ LMCT which has no intensity in a planar conformation. The prime refers to the local coordinate system of the phenolate oxygen atom (see below).

The spectrum of the monooxidized cation **2⁺** shows some significant changes compared to the spectrum of **2** (Figure 7). Thus, while the d–d transition exhibits nearly no change (inset of Figure 7) the charge-transfer transitions exhibit strong differences. The main change is a shift of the 30200-cm^{-1} band in **2** to 32300 cm^{-1} with a decrease of its

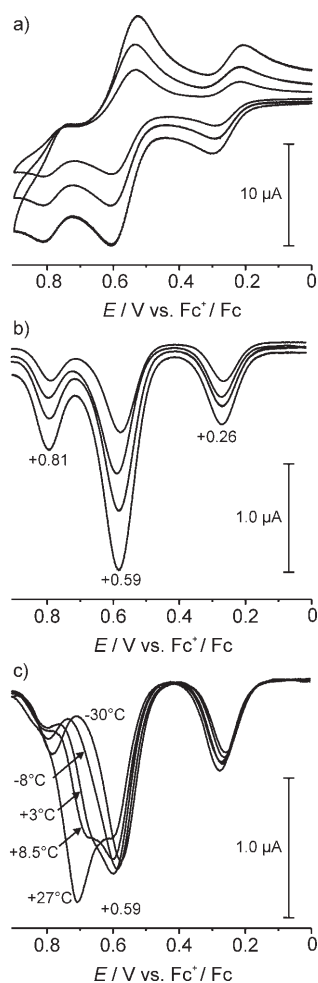


Figure 5. a) Cyclic voltammograms of **2** in CH_2Cl_2 at -30°C (scan rates: 100, 200, 400 mV s^{-1}); b) square-wave voltammograms of **2** at -30°C (frequencies: 6, 12, 25, 50 Hz); c) square-wave voltammograms of **2** in CH_2Cl_2 at temperatures from $+27$ to -30°C (frequency: 40 Hz).

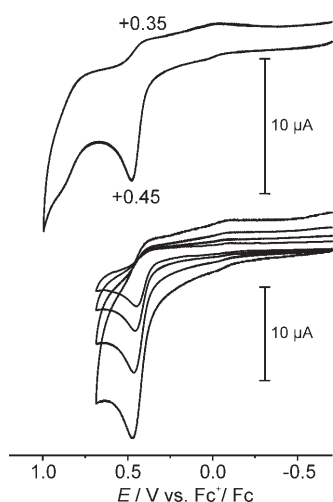


Figure 6. Cyclic voltammograms of **3** in CH_2Cl_2 (scan rates: 100 mV s^{-1} (top); 50, 100, 200, 400 mV s^{-1} (bottom)) at ambient temperature.

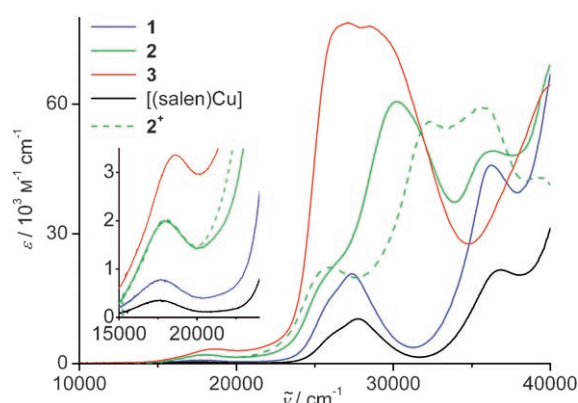


Figure 7. Electronic absorption spectra of **1** (CH_2Cl_2), **2** (CH_2Cl_2), **3** (DMF), and $[(\text{salen})\text{Cu}^{\text{II}}]$ (CH_3CN) at ambient temperature. The spectrum of $\mathbf{2}^+$, which was generated by addition of one equivalent of $[(\text{C}_6\text{H}_4\text{Br})_3\text{N}][\text{SbCl}_6]$ to a solution of **2** in CH_2Cl_2 at -40°C , is corrected for the absorption of the reduced amine. The inset shows the region of the d-d transitions.

intensity. The bands that appear as a shoulder at around 27000 cm^{-1} are shifted to slightly lower energy with a maximum at 25900 cm^{-1} with slightly higher intensity.

The spectrum of **3** shows very intense transitions between 24000 and 35000 cm^{-1} as in the corresponding Ni complex. These transitions are solely due to the nitrobenzene chromophore and prevent the analysis of the phenolate-Cu chromophores.

Magnetic measurements: We performed temperature-dependant measurements of the magnetic susceptibility (SQUID, 2–300 K, 1.0 T) of samples of **2b**, **2c**, **2e**, and **3**. The effective magnetic moment μ_{eff} of all samples increases upon lowering the temperature, in agreement with the expected ferromagnetic interactions via the spin-polarization mechanism (Figure 8). μ_{eff} decreases below 5 K due to weak intermolecular antiferromagnetic interactions and saturation effects. The data for **2c** reveal a step in μ_{eff} at around 190 K. Measurements on different batches of **2c** were performed after extensive purge-and-thaw cycles in the magnetometer to ensure that this step is not caused by molecular oxygen absorbed on the crystallite surfaces. All these measurements revealed the same behavior, thereby indicating that this is an inherent property of **2c**, which we assign to a structural phase-transition.

In order to obtain the coupling constants (J) we simulated the temperature dependence of μ_{eff} with the appropriate spin-Hamiltonian [Eq. (1)] for an equilateral Cu^{II}_3 ($S_i=1/2$) triangle by a full-matrix diagonalization approach including Heisenberg-Dirac-van Vleck (HDvV) exchange and a Zeeman interaction using the program package JulX 1.2.1,^[92] which takes saturation effects into account. Intermolecular interactions were modeled by inclusion of a Weiss temperature θ .

$$H = -2J(S_1S_2 + S_2S_3 + S_1S_3) + \sum_{i=1}^3 [g_i\mu_B S_i B] \quad (1)$$

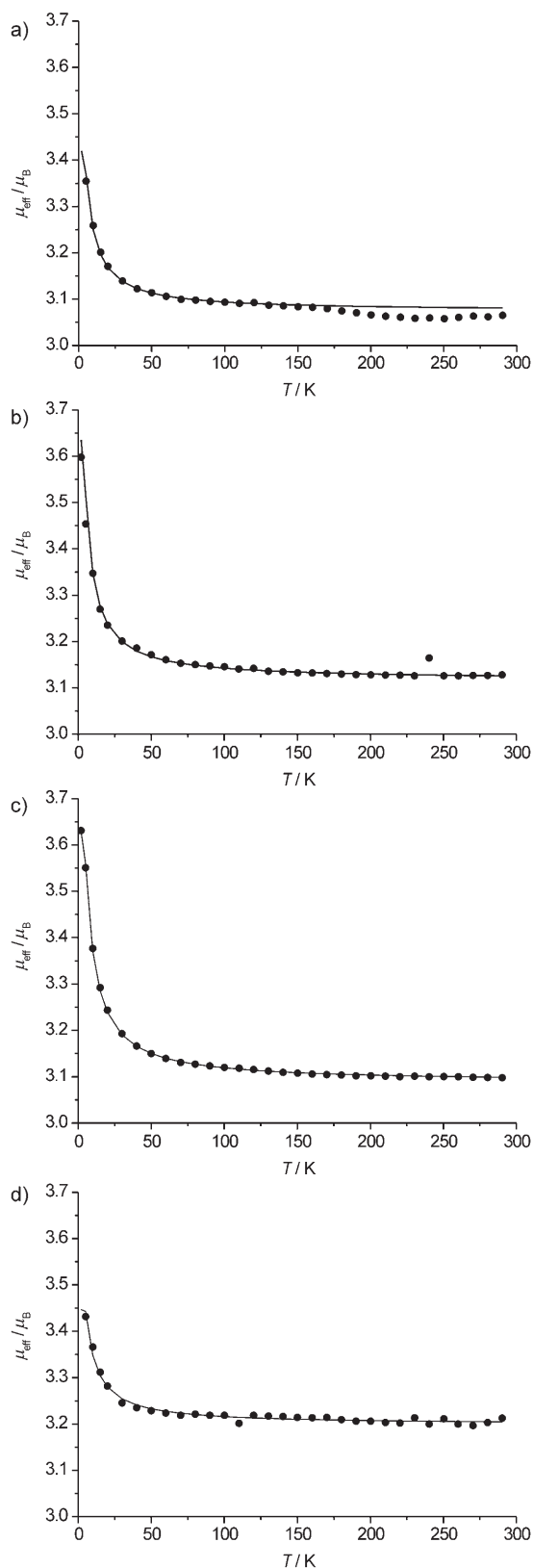


Figure 8. Temperature dependence of μ_{eff} for **2c** (a), **2b** (b), **2e** (c), and **3** (d). The solid lines correspond to the best fits: **2c**: $J = +1.08 \text{ cm}^{-1}$, $g = 2.049$, $\chi_{\text{TIP}} = 100 \times 10^{-6} \text{ cm}^3 \text{ mol}^{-1}$, and $\theta = -0.26 \text{ K}$; **2b**: $J = +1.17 \text{ cm}^{-1}$, $g = 2.078$, $\chi_{\text{TIP}} = 380 \times 10^{-6} \text{ cm}^3 \text{ mol}^{-1}$, and $\theta = -0.07 \text{ K}$; **2e**: $J = +1.55 \text{ cm}^{-1}$, $g = 2.055$, $\chi_{\text{TIP}} = 169 \times 10^{-6} \text{ cm}^3 \text{ mol}^{-1}$, and $\theta = -0.10 \text{ K}$; **3**: $J = +1.02 \text{ cm}^{-1}$, $g = 2.132$, $\chi_{\text{TIP}} = 272 \times 10^{-6} \text{ cm}^3 \text{ mol}^{-1}$, and $\theta = -0.37 \text{ K}$. The values for χ_{TIP} have been extracted from the experimental and theoretical data.

Fitting of the data (floating J , g , θ) indicated a covariance of J and θ and a nonperfect reproduction of the curvature was obtained. Uncertainties in the exact molar composition are all incorporated in the value of g but do not affect the value of J , therefore any differences in the values of g should not be considered as being due to changes in the electronic structure of the complexes. We also performed careful simulations of the data, paying special attention to the curvature of the μ_{eff} versus T plots in the area of strongest slope (between 20 and 80 K) to obtain relatively accurate J values. In this approach, even small variations in J change the simulations significantly. To obtain an insight into the accuracy of the J values, we then performed simulations with slightly different J values and found that increasing (decreasing) the J value leads to a small overall increase (decrease) of μ_{eff} over the whole temperature range. We therefore reevaluated the g value by fitting the data above 130 K for each specific value of J . Figure S1 (see Supporting Information) summarizes the results of this procedure for compound **2e**. Whereas the curve for $J = 1.55 \text{ cm}^{-1}$ fits the μ_{eff} values, especially the curvature, perfectly, the curves for $J = 1.40$ and 1.70 cm^{-1} lie below and above the experimental data, respectively. We therefore estimate an error for the J value of $\pm 0.10 \text{ cm}^{-1}$. Note that the covariance of J and θ was also suppressed. The best J values obtained by this procedure are $J = (+1.08 \pm 0.10) \text{ cm}^{-1}$ for **2c**, $J = (+1.17 \pm 0.10) \text{ cm}^{-1}$ for **2b**, $J = (+1.55 \pm 0.10) \text{ cm}^{-1}$ for **2e**, and $J = (+1.02 \pm 0.10) \text{ cm}^{-1}$ for **3**. The J value for **1** was found to be $(+1.52 \pm 0.10) \text{ cm}^{-1}$.^[23]

Discussion

Influence of the substituents on the electrochemical properties: The electrochemistry of mononuclear Cu salen complexes has been studied intensively.^[100,101,104,110,112] The parent complex [(salen)Cu] and its ketimine derivative [(Me₂salen)Cu] are oxidized irreversibly at 0.60 and 0.53 V, respectively,^[101] and this irreversibility has been ascribed to an electrochemical oxidative polymerization at the electrode surface through the *para* position of the phenol unit. While this oxidation was supposed to involve the initial formation of a Cu^{III} species, charge delocalization is thought to be sufficient to allow an oxidative coupling mainly in the *para* position. The introduction of substituents in the *ortho* and *para* positions inhibits this radical chemistry and leads to a reversible oxidation process, namely two reversible oxidations at 0.45 and 0.65 V for [(salen')Cu] and 0.55 and 0.75 V for [(salen^{tBu2})Cu].^[112] These two oxidations have been assigned to the successive formation of a Cu^{II} phenoxyl and a Cu^{II} bisphenoxyl radical species for both complexes.

The irreversible oxidation of the unsubstituted trinuclear complex **1** at +0.61 V is in accordance with the irreversible oxidation of [(salen)Cu] at +0.60 V, thereby implying a redox polymerization of the trinuclear complexes at the electrode surface. In this respect, there are no striking differences between the trinuclear triplesalen complex and its

mononuclear salen analogues. In contrast, a strong cathodic shift of the first oxidation of the *tert*-butyl-substituted complex **2** to +0.26 V is observed in comparison to [(salen')Cu] and [(salen^{tbu})Cu], which indicates a substantial stabilization of the oxidized species in the trinuclear complex. The introduction of two *tert*-butyl groups (i.e. going from [(salen)Cu] to [(salen^{tbu})Cu]) stabilizes the oxidized species by 50 mV.^[112] Furthermore, substitution of the ethylenediamine bridge by a cyclohexanediamine bridge results in an overall stabilization of 150 mV.^[110] This implies a cathodic shift due to two *tert*-butyl substituents in the range of 50–150 mV. However, the stabilization on going from **1** to **2** (350 mV) implies that an additional stabilizing effect is operative in monooxidized **2**⁺. Further evidence for an extra stabilization of **2**⁺ arises from the increase of the peak separation to the second oxidation, which is 330 mV in **2** and only 200 mV in [(salen^{tbu})Cu] and [(salen')Cu].

The oxidized species **2**⁺ is inherently a mixed-valent species as a metal-centered oxidation to a Cu^{III} species would yield a mixed-valent Cu^{III}Cu^{II}Cu^{II} species. For a ligand-oxidized radical species three terminal phenolates and one central phloroglucinol moiety might be oxidized. The trinuclear Ni triplesalen complexes are a good reference for understanding the electronic structure of monooxidized **2**⁺, and we have shown by EPR spectroscopy that the monooxidized trinuclear Ni complexes exhibit valence tautomerism.^[65] They display two sub-spectra in the EPR spectrum at 10 K, one of which is due to a ligand-oxidized radical species and one to a metal-oxidized Ni^{III} species. These sub-spectra and their relative ratios are virtually identical for [(tal-en^{tbu})Ni₃]⁺ and [(tal-en^{NO₂})Ni₃]⁺. Oxidation of a terminal *tert*-butyl-containing phenolate in the former and an NO₂-containing phenolate in the latter would lead to differences in the radical EPR sub-spectra, especially in the relative ratio of these sub-spectra. We therefore assigned the oxidized radical species as being formed by oxidation of the central phloroglucinol units. It is interesting to note that the oxidation of phloroglucinol is 0.24 V easier than for phenol.^[113] The intensity of the radical EPR signal of [(tal-en^{tbu})Ni₃]⁺ decreases reversibly upon increasing the temperature, and at 100 K only the Ni^{III} EPR species is detected. The concomitant detection of both valence tautomers (radical and Ni^{III} species) indicates that these pairs of valence tautomers have similar energies. The temperature dependence of the equilibrium is considered to be entropy driven. The entropy gain associated with the Ni^{III} species can be attributed to the threefold degeneracy, which implies that the mixed-valent Ni^{III}Ni^{II}Ni^{II} species is of class II.^[114] Along the same lines, the non-degeneracy of the radical species can be assigned to the oxidation of a central (phloroglucinol) phenolate species which is delocalized over all three sides (class III).

While the ligand-oxidized radical species and the metal-oxidized Ni^{III} species in the trinuclear Ni complexes are close in energy, the higher effective nuclear charge of Cu^{II} compared to Ni^{II} (see above) should result in a ligand-oxidized radical species for the trinuclear Cu triplesalen com-

plexes, in agreement with the assignment for the singly and doubly oxidized mononuclear salen-type Cu complexes.^[110,112]

The UV/Vis spectra exhibit nearly no change in the d–d transition upon going from **2** to **2**⁺, thereby proving that the oxidation is not Cu centered. Additionally, the potential phenolate O p_z→Cu^{II} d_{x²-y²} LMCT transition at 30 200 cm⁻¹ in **2**, which gains intensity from the ligand folding at the central phenolate (see above), increases in energy upon oxidation with a concomitant decrease in intensity. This is in agreement with a simple description whereby the redox-active orbital comprises of the whole central phloroglucinol unit incorporating all three phenolate donors. Oxidation leads to an energy stabilization of the oxygen orbitals and thus a shift of the LMCT to higher energies with reduced intensity due to a reduced bonding interaction (increased energy separation and reduced resonance integral). This redox-active orbital also comprises, although to a lower extent, some C=N double bond character from the ketimine units, which contributes to the overall conjugated system. This results in the reduced energy of the Cu^{II}→C=N π* MLCT transition observed in **2**⁺, and the increase in intensity, due to a decrease in the energy separation between the orbitals involved. We can therefore assign the oxidized species **2**⁺ to an oxidation of the central phloroglucinol unit. The extra energetic stabilization of this monocation may be ascribed to a class III delocalization^[114] of the central phenoxyl radical Cu^{II} species over all three phenolate Cu^{II} sites.

The irreversible oxidation of **3** at +0.45 V might be due to an oxidation-induced decomplexation, which supports the critical effect of the terminal substituents on the electronic structures of the trinuclear Cu complexes.

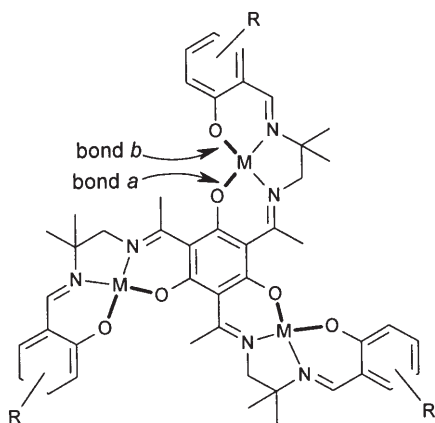
Electronic and structural effects on the spin-polarization:

As summarized in the introduction, the concept of spin-polarization, which is almost always working in organic chemistry, cannot be applied in a straightforward manner to transition metal complexes. In this respect, our series of trinuclear Cu^{II} triplesalen complexes with different terminal substituents, as well as the changes in the relative orientations of the magnetic orbitals with the plane of the bridging benzene ring, are well suited to obtaining more experimental insight into the spin-polarization mechanism in transition metal complexes.

Several theoretical investigations have been performed to understand the differences between the spin-polarization in organic radicals and carbenes and transition metal complexes.^[34,115–117] Karafiloglou already showed for organic diradicals that not only the spin-polarization and exchange and superexchange interactions contribute to the overall coupling.^[118] Analogously, Cano et al. have emphasized the contribution of both spin-polarization and spin-delocalization in transition metal complexes.^[119] This has also been demonstrated for resorcinol- and hydroquinone-bridged dinuclear Mo^V complexes by Bencini et al.,^[120] who showed that the orientation of the magnetic orbital on each metal site relative to the plane of the bridging benzene ring is crucial for a ferromagnetic or antiferromagnetic contribution to the su-

perexchange interaction as well as to the spin-polarization mechanism.

In our previous study of trinuclear nickel triplesalen complexes^[65] we established that communication between the nickel salen subunits is influenced by the terminal substituents on the phenol moieties. As the electronic communication between the three metal ions is mediated by the central metal–phenolate bonds (bonds *a* in Scheme 4), the strengthening of these bonds should increase the interaction between the metal ions. An indirect method for influencing



Scheme 4.

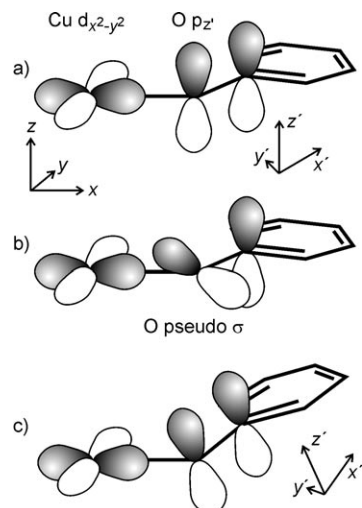
these central metal–phenolate bonds is provided by varying the strengths of the terminal metal–phenolate bonds (bond *b* in Scheme 4). In accordance with Pauling's electroneutrality principle, a weakening of the terminal bonds *b* (less charge donation from the terminal phenolates) would strengthen the central bonds *a* (more charge donation from the central phenolates), and vice versa.^[121] In this respect, we have found that the introduction of *tert*-butyl groups in [(tal-en^{tBu2})Ni₃] leads to stronger bonds *b* and weaker bonds *a* than in [(tal-en)Ni₃], whereas the nitro groups in [(tal-en^{NO2})Ni₃] result in weaker bonds *b* and thus stronger bonds *a*.

We have also envisioned a second modulating effect induced by the ligand folding which opposes the electronic control described above. The degree of ligand folding, which shows the strongest effect at the central phenolate units, increases in the order [(tal-en^{NO2})Ni₃] < [(tal-en)Ni₃] < [(tal-en^{tBu2})Ni₃].

The trinuclear copper triplesalen complexes provide a good tool for investigating the interplay between electronic and structural effects due to the paramagnetic nature of the Cu^{II} ions. In the hypothetical limit of a frozen ligand folding irrespective of the nature of the terminal substituents, the *tert*-butyl substituents in **2** are expected to strengthen bonds *b*, thereby resulting in weaker bonds *a* and thus in a decrease of the strength of the exchange coupling. (The exchange coupling constant *J* is proportional to the square of the covalency.)^[14] On the other hand, introduction of the nitro substituent in **3** should decrease the strength of

bonds *b* and therefore increase the strength of bonds *a*, therefore the exchange coupling should follow the trend **3** > **1** > **2**. However, the experimental trend, as established by magnetic measurements, is **1** ≈ **2e** > **2b** > **2c** > **3**. The coupling constant for the *tert*-butyl substituted complexes **2** in crystals of **2c** and **2b** is smaller ($J \approx 1.1$ – 1.2 cm^{-1}) than for crystals of **2e** ($J = 1.55 \text{ cm}^{-1}$), the value for which is close to the value for the unsubstituted complex **1**.^[23] Interestingly, the value of *J* for the nitro complex **3** is even lower than that for **1** and **2**.

The starting point for our discussion is the commonly accepted assumption that the spin-polarization in *meta*-phenylene-bridged radicals and carbenes follows a π mechanism.^[24,120] In this respect, an efficient spin-polarization in phloroglucinol-bridged transition metal complexes through the π orbitals of the central benzene ring requires a high spin-density in the p_z orbitals of the coordinated oxygen atoms. In a coplanar orientation of the CuO₂N₂ plane and the plane of the phloroglucinol unit (coplanarity of the *xy* plane of the salen subunit and the *x'y'* plane of phloroglucinol; Scheme 5 a) the magnetic Cu $d_{x^2-y^2}$ orbital and the O p_z



Scheme 5. Orientation of the oxygen p orbitals in copper salen complexes with planar and bowl-shaped geometries. See text for details.

orbital (the π orbital with regard to the O–C^{benzene} bond) are orthogonal and the overlap integral is zero (Scheme 5 a), which means that no spin-delocalization occurs by this bonding pathway. The Cu–O bond and the spin density on the oxygen atom originate from the pseudo- σ overlap of the Cu $d_{x^2-y^2}$ orbital with the O p_y orbital (Scheme 5 b). Pseudo- σ here reflects the nonlinearity of the local *x* axis of the CuO₂N₂ coordinate system and the *y'* axis of the phloroglucinol coordinate system.^[121,122] The positive spin-density in the O p_y orbital spin-polarizes the remaining oxygen orbitals involving the O p_z orbital.^[119] The detour via the pseudo- σ bond therefore results in only an indirect spin-polarization pathway.

Folding at the central Cu^{II}–phenolate bond (noncoplanarity of the *xy* and *x'y'* planes; Scheme 5 c) results in a nonor-

thogonal overlap of the O p_z orbital with the magnetic Cu $d_{x^2-y^2}$ orbital and therefore to a direct delocalization of spin density into the O p_z orbital, which results in a direct spin-polarization pathway. This higher spin density in the O p_z orbitals should result in a stronger spin-polarization through the central benzene ring as compared to the coplanar arrangement described above.

We have performed density functional calculations for the quartet ground-state in order to quantify these qualitative considerations. Since we are only interested in the variations of the spin densities induced by ligand folding at the central Cu^{II}-phenolate bond, we used simplified models of the complexes for our calculations. These models consist of the parent phloroglucinol bridging unit with three coordinated Cu^{II} ions. The central ketimine groups are modeled by N=CH units while the terminal phenolate and aldimine donors are modeled by OH⁻ anions and NH₃ groups, respectively. The ligand folding is mimicked by rotation of the CuO₂N₂ planes about either the central O-N vector or the Cu-O vector. We calculated several model geometries. One structure had all atoms (except the hydrogen atoms) lying exactly in one plane whereas the others were closer to the experimentally obtained molecular structures with slight deviations at the ketimine carbon atoms. Ligand folding opens a direct bonding pathway between the Cu $d_{x^2-y^2}$ orbital and the O p_z orbital in all cases, as evidenced by an increased spin density in the O p_z orbital. However, a close inspection of the atomic spin-densities of the central benzene ring and the distribution of the spin densities of the p_x , p_y , and p_z orbitals demonstrates that the spin-polarization and the spin-delocalization increase due to the ligand folding. The spin-densities for two similar model structures are shown in Figure 9. The structure in Figure 9a is folded by rotation

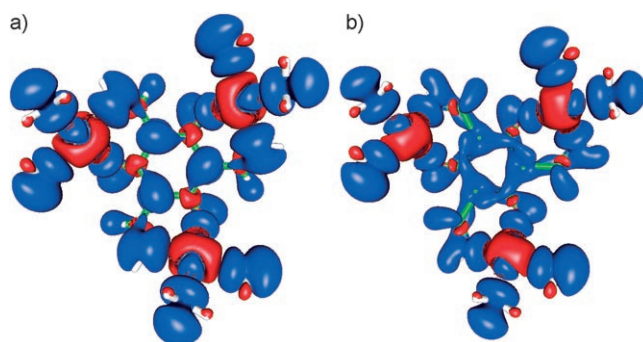


Figure 9. The spin-densities for two different model structures show a) spin-polarization or b) spin-delocalization on the central benzene ring.

about the Cu-O bond while the geometry in Figure 9b is obtained by rotation around the O-N vector. The structure in Figure 9a shows an increase of the absolute atomic and p_z spin-densities of alternating signs in the central benzene ring, while for the similar geometry in Figure 9b an overall increase of positive spin-densities is observed at all carbon atoms. These findings are consistent with the above-mentioned theoretical publications,^[118-120] which reveal that both

spin-polarization and spin-delocalization contribute to the overall coupling between transition metal ions. Thus, assigning the experimentally observed strong ferromagnetic coupling in the folded molecular structures to spin-polarization or spin-delocalization is not justified. The effects of the d^n electronic configuration on the interplay between spin-polarization and spin-delocalization will be studied by using trinuclear transition metal complexes with other transition metal ions.

It is interesting to compare these results with the famous exception to *meta*-phenylene-bridged organic radicals, namely 4,6-dimethoxy-1,3-phenylenebis(*N*-*tert*-butyl nitroxide). This *meta*-phenylene-bridged diradical has a singlet ground-state while all other known *meta*-phenylene-bridged radicals and carbenes possess a triplet ground-state.^[123] The molecular structure established by X-ray diffraction shows that the nitroxide moieties lie out of the plane of the *meta*-phenylene bridge (65.1° and 75.3°). Thus, the nitroxide SOMOs are almost orthogonal to the π system of the bridging phenylene unit. This leads to an indirect spin-polarization pathway that is less effective than the superexchange (spin-delocalization) contributions, which are antiferromagnetic.

The ligand system based on *N,N',N''*-1,3,5-benzenetris(oxamate), which is closely related to our triplesalen ligand system, provides another good point of comparison.^[51-55] The coupling constant for the trinuclear Cu^{II} complex of the parent ligand was found to be +5.8 cm⁻¹.^[52] It is interesting to speculate about the origin of the stronger ferromagnetic coupling in this *meta*-phenylene-bridged complex. The amide coordination to Cu^{II} rather than the phenolate coordination in the triplesalen ligands results in a stronger covalency of the metal-ligand bond, which gives rise to stronger exchange interactions. Moreover, the basal plane of the copper in the tris(oxamate) complex is almost perpendicular to the plane of the bridging benzene moiety. This leads to strong π interactions between the Cu $d_{x^2-y^2}$ orbitals and the benzene ring, which allows for direct spin-polarization as compared to the indirect spin-polarization effects operating in 1-3.

Conclusions

We have synthesized a series of trinuclear Cu^{II} triplesalen complexes with varying terminal substituents (H, NO₂, *tert*-butyl). These trinuclear complexes are not flat and show severe ligand folding. This ligand folding is stronger at the central Cu^{II}-phenolate bonds than at the terminal Cu^{II}-phenolate bonds. The different molecular structures obtained for **2** in various solvates show different degrees of ligand folding, ranging from low non-uniform ligand folding to strong uniform ligand folding, the latter of which leads to bowl-shaped molecular structures. These bowl-shaped structures can be either a molecular property or stabilized by intermolecular interactions, as found in the supermolecular aggregate **2**₂·2CH₂Cl₂. This supramolecular structure consists

of two bowl-shaped units which form a disk that incorporates two CH_2Cl_2 molecules like two pearls in an oyster and is stabilized by weak van der Waals forces.

Copper salen complexes catalyze a number of reactions,^[124–126] such as the asymmetric synthesis of α -methyl- α -amino acids.^[127–131] Folding of the salen ligand and especially of the diamine bridge has been found to be essential for the enantioselectivity of these catalytic reactions. We are currently investigating the cooperative reactivity between the three copper centers in these reactions and we are also trying to synthesize a chiral triplesalen ligand from enantiomerically pure diimine moieties.

The exchange interactions in all trinuclear copper triplesalen complexes are ferromagnetic, as expected for a *meta*-phenylene bridging unit due to the spin-polarization mechanism. In principle, the exchange coupling can be mediated by the different terminal ligand substituents, with electron-donating groups stabilizing the terminal Cu^{II} -phenolate bond *b* (Scheme 4), which leads to weaker central Cu^{II} -phenolate bonds *a*, and vice versa. However, this effect of the terminal substituent seems to be small and is partially obscured by the effects of the ligand folding. Flat geometries weaken the coupling while ligand folding strengthens the coupling. Density functional calculations indicate that this effect cannot be ascribed only to spin-polarization and that spin-delocalization is also effective.

The electrochemical characterization has established three reversible oxidation steps for **2**. A comparison with various mononuclear salen Cu complexes shows a significant stabilization of the mono-oxidized species $\mathbf{2}^+$, which has been generated chemically and studied by electron absorption spectroscopy. This oxidation is ligand-centered and leads to a phenoxy radical species. In analogy to the trinuclear nickel triplesalen complexes and based on oxidation potentials of phloroglucinol versus phenol, this oxidation is assigned to the central phloroglucinol unit. Delocalization of the phenoxy radical over three phenolate- Cu^{II} sites leads to an extra stabilization of the mono-oxidized species in the triplesalen complex as compared to mononuclear salen complexes.

Direct interaction of the central phloroglucinol-based radical spin with the coordinated Cu^{II} spin centers should lead to strong exchange interactions. This interaction could be either ferromagnetic or antiferromagnetic for other metal ions depending on the d^n electron configuration of the coordinated metal ion (a ferromagnetic coupling is most likely for Cu^{II}). However, this coupling scheme should provide energetically well isolated high-spin ground-states for metal ions with local spin states, S_i , greater than 1/2 even for antiferromagnetic interactions.

Acknowledgment

This work was supported by the Fonds der Chemischen Industrie, the BMBF, the Dr. Otto Röhm Gedächtnisstiftung, and the DFG (SFB 424).

- [1] J. S. Miller, J. C. Calabrese, A. J. Epstein, R. W. Bigelow, J. H. Zhang, W. M. Reiff, *J. Chem. Soc. Chem. Commun.* **1986**, 1026–1028.
- [2] J. S. Miller, J. C. Calabrese, H. Rommelmann, S. Chittipeddi, A. J. Epstein, J. H. Zhang, W. M. Reiff, *J. Am. Chem. Soc.* **1987**, *109*, 769–781.
- [3] J. S. Miller, *Inorg. Chem.* **2000**, *39*, 4392–4408.
- [4] T. Lis, *Acta Crystallogr. Sect. B* **1980**, *36*, 2042–2046.
- [5] G. Christou, D. Gatteschi, D. N. Hendrickson, R. Sessoli, *MRS Bull.* **2000**, *25*, 66–71.
- [6] J. R. Long in *Chemistry of Nanostructured Materials* (Ed.: P. Yang), World Scientific, Hong Kong, **2003**, p. 291–315.
- [7] D. Gatteschi, R. Sessoli, *Angew. Chem.* **2003**, *115*, 278–309; *Angew. Chem. Int. Ed.* **2003**, *42*, 268–297.
- [8] D. Gatteschi, R. Sessoli, J. Villain, *Molecular Nanomagnets*, Oxford University Press, Oxford, **2006**.
- [9] R. Sessoli, D. Gatteschi, A. Caneschi, M. A. Novak, *Nature* **1993**, *365*, 141–143.
- [10] R. Sessoli, H. L. Tsai, A. R. Schake, S. Y. Wang, J. B. Vincent, K. Folting, D. Gatteschi, G. Christou, D. N. Hendrickson, *J. Am. Chem. Soc.* **1993**, *115*, 1804–1816.
- [11] O. Kahn, *Acc. Chem. Res.* **2000**, *33*, 647–657.
- [12] C. Zener, *Phys. Rev.* **1951**, *82*, 403–405.
- [13] G. Blondin, J.-J. Girerd, *Chem. Rev.* **1990**, *90*, 1359–1376.
- [14] T. Glaser, K. Rose, S. E. Shadle, B. Hedman, K. E. Hodgson, E. I. Solomon, *J. Am. Chem. Soc.* **2001**, *123*, 442–454.
- [15] T. Glaser, T. Beissel, E. Bill, T. Weyhermüller, V. Schünemann, W. Meyer-Klaucke, A. X. Trautwein, K. Wieghardt, *J. Am. Chem. Soc.* **1999**, *121*, 2193–2208.
- [16] L. F. Chibotaru, J.-J. Girerd, G. Blondin, T. Glaser, K. Wieghardt, *J. Am. Chem. Soc.* **2003**, *125*, 12615–12630.
- [17] J. Kanamori, *J. Phys. Chem. Solids* **1959**, *10*, 87–98.
- [18] O. Kahn, *Inorg. Chim. Acta* **1982**, *62*, 3–14.
- [19] T. Glaser, H. Theil, I. Liratzis, T. Weyhermüller, E. Bill, *Inorg. Chem.* **2006**, *45*, 4889–4891.
- [20] H. C. Longuet-Higgins, *J. Chem. Phys.* **1950**, *18*, 265–274.
- [21] H. M. McConnell, *J. Chem. Phys.* **1963**, *39*, 1910.
- [22] T. Glaser, M. Gerenkamp, R. Fröhlich, *Angew. Chem.* **2002**, *114*, 3984–3986; *Angew. Chem. Int. Ed.* **2002**, *41*, 3823–3825.
- [23] T. Glaser, M. Heidemeier, S. Grimme, E. Bill, *Inorg. Chem.* **2004**, *43*, 5192–5194.
- [24] H. Iwamura, *Adv. Phys. Org. Chem.* **1990**, *26*, 179–253.
- [25] A. Rajca, *Chem. Eur. J.* **2002**, *8*, 4834–4841.
- [26] K. Yoshizawa, R. Hoffmann, *J. Am. Chem. Soc.* **1995**, *117*, 6921–6926.
- [27] H. Iwamura, N. Koga, *Acc. Chem. Res.* **1993**, *26*, 346–351.
- [28] D. A. Dougherty, *Acc. Chem. Res.* **1991**, *24*, 88–94.
- [29] A. A. Ovshinnikov, *Theor. Chim. Acta* **1978**, *47*, 297–304.
- [30] S.-i. Mitsubori, T. Ishida, T. Nogami, H. Iwamura, *Chem. Lett.* **1994**, 285–288.
- [31] F. Lloret, G. De Munno, M. Julve, J. Cano, R. Ruiz, A. Caneschi, *Angew. Chem.* **1998**, *110*, 143–145; *Angew. Chem. Int. Ed.* **1998**, *37*, 135–138.
- [32] T. Ishida, K. Nakayama, M. Nakagawa, W. Sato, Y. Ishikawa, *Synth. Met.* **1997**, *85*, 1655–1658.
- [33] T. Ishida, S.-i. Mitsubori, T. Nogami, N. Takeda, M. Ishikawa, H. Iwamura, *Inorg. Chem.* **2001**, *40*, 7059–7064.
- [34] T. Ishida, T. Kawakami, S.-i. Mitsubori, T. Nogami, K. Yamaguchi, H. Iwamura, *J. Chem. Soc. Dalton Trans.* **2002**, 3177–3186.
- [35] K. Nakayama, T. Ishida, R. Takayama, D. Hashizume, M. Yasui, F. Iwasaki, T. Nogami, *Chem. Lett.* **1998**, 497–498.
- [36] R. Feyerhem, S. Abens, D. Günther, T. Ishida, M. Meißner, M. Meschke, T. Nogami, M. Steiner, *J. Phys. Condens. Matter* **2000**, *12*, 8495–8509.
- [37] J. Omata, T. Ishida, D. Hashizume, F. Iwasaki, T. Nogami, *Inorg. Chem.* **2001**, *40*, 3954–3958.
- [38] T. Kusaka, T. Ishida, D. Hashizume, F. Iwasaki, T. Nogami, *Chem. Lett.* **2000**, 1146–1147.

- [39] D. R. Corbin, L. C. Francesconi, D. N. Hendrickson, G. D. Stucky, *Inorg. Chem.* **1981**, *20*, 2084–2089.
- [40] M. Ruben, J. Rojo, F. J. Romero-Salguero, L. H. Uppadine, J.-M. Lehn, *Angew. Chem.* **2004**, *116*, 3728–3747; *Angew. Chem. Int. Ed.* **2004**, *43*, 3644–3662.
- [41] B. F. Fieselmann, D. N. Hendrickson, G. D. Stucky, *Inorg. Chem.* **1978**, *17*, 1841–1848.
- [42] L. C. Francesconi, D. R. Corbin, D. N. Hendrickson, G. D. Stucky, *Inorg. Chem.* **1979**, *18*, 3074–3080.
- [43] H. Oshio, *J. Chem. Soc. Chem. Commun.* **1991**, 240–241.
- [44] H. Oshio, H. Ichida, *J. Phys. Chem.* **1995**, *99*, 3294–3302.
- [45] J. A. McCleverty, M. D. Ward, *Acc. Chem. Res.* **1998**, *31*, 842–851.
- [46] A. M. W. Cargill Thompson, D. Gatteschi, J. A. McCleverty, J. A. Navas, E. Rentschler, M. D. Ward, *Inorg. Chem.* **1996**, *35*, 2701–2703.
- [47] S. R. Bayly, E. R. Humphrey, H. de Chair, C. G. Paredes, Z. R. Bell, J. C. Jeffery, J. A. McCleverty, M. D. Ward, F. Totti, D. Gatteschi, S. Courric, B. R. Steele, C. G. Screttas, *J. Chem. Soc. Dalton Trans.* **2001**, 1401–1414.
- [48] V. A. Ung, A. Thompson, D. A. Bardwell, D. Gatteschi, J. C. Jeffery, J. A. McCleverty, F. Totti, M. D. Ward, *Inorg. Chem.* **1997**, *36*, 3447–3454.
- [49] V. A. Ung, S. M. Couchman, J. C. Jeffery, J. A. McCleverty, M. D. Ward, F. Totti, D. Gatteschi, *Inorg. Chem.* **1999**, *38*, 365–369.
- [50] S. R. Bayly, J. A. McCleverty, M. D. Ward, D. Gatteschi, F. Totti, *Inorg. Chem.* **2000**, *39*, 1288–1293.
- [51] I. Fernández, R. Ruiz, J. Faus, M. Julve, F. Lloret, J. Cano, X. Ottenwaelder, Y. Journaux, C. Muñoz, *Angew. Chem.* **2001**, *113*, 3129–3132; *Angew. Chem. Int. Ed.* **2001**, *40*, 3039–3042.
- [52] X. Ottenwaelder, J. Cano, Y. Journaux, E. Rivière, C. Brennan, M. Nierlich, R. Ruiz-García, *Angew. Chem.* **2004**, *116*, 868–870; *Angew. Chem. Int. Ed.* **2004**, *43*, 850–852.
- [53] E. Pardo, I. Morales-Osorio, M. Julve, F. Lloret, J. Cano, R. Ruiz-García, J. Pasan, C. Ruiz-Pérez, X. Ottenwaelder, Y. Journaux, *Inorg. Chem.* **2004**, *43*, 7594–7596.
- [54] E. Pardo, K. Bernot, M. Julve, F. Lloret, J. Cano, R. Ruiz-García, J. Pasán, C. Ruiz-Pérez, X. Ottenwaelder, Y. Journaux, *Chem. Commun.* **2004**, 920–921.
- [55] C. L. M. Pereira, E. F. Pedroso, H. O. Stumpf, M. A. Novak, L. Ricard, R. Ruiz-García, E. Rivière, Y. Journaux, *Angew. Chem.* **2004**, *116*, 974–976; *Angew. Chem. Int. Ed.* **2004**, *43*, 956–958.
- [56] A. R. Paital, T. Mitra, D. Ray, W. T. Wong, J. Ribas-Ariño, J. J. Novoa, J. Ribas, G. Aromi, *Chem. Commun.* **2005**, 5172–5174.
- [57] T. Glaser, M. Heidemeier, T. Lügger, *Dalton Trans.* **2003**, 2381–2383.
- [58] B. J. Kennedy, K. S. Murray, *Inorg. Chem.* **1985**, *24*, 1552–1557.
- [59] S. Mitra, *Prog. Inorg. Chem.* **1977**, *22*, 309–408.
- [60] A. Bencini, I. Ciofini, M. G. Uytterhoeven, *Inorg. Chim. Acta* **1998**, *274*, 90–101.
- [61] W. Zhang, E. N. Jacobsen, *J. Org. Chem.* **1991**, *56*, 2296–2298.
- [62] K. A. Campbell, M. R. Lashley, J. K. Wyatt, M. H. Nantz, R. D. Britt, *J. Am. Chem. Soc.* **2001**, *123*, 5710–5719.
- [63] J. Krzystek, J. Telsner, *J. Magn. Reson.* **2003**, *162*, 454–465.
- [64] H. Miyasaka, R. Clerac, W. Wernsdorfer, L. Lecren, C. Bonhomme, K.-i. Sugiura, M. Yamashita, *Angew. Chem.* **2004**, *116*, 2861–2865; *Angew. Chem. Int. Ed.* **2004**, *43*, 2801–2805.
- [65] T. Glaser, M. Heidemeier, R. Fröhlich, P. Hildebrandt, E. Bothe, E. Bill, *Inorg. Chem.* **2005**, *44*, 5467–5482.
- [66] T. Glaser, M. Heidemeier, T. Weyhermüller, R.-D. Hoffmann, H. Rupp, P. Müller, *Angew. Chem.* **2006**, *118*, 6179–6183; *Angew. Chem. Int. Ed.* **2006**, *45*, 6033–6037.
- [67] T. Glaser, M. Heidemeier, R. Fröhlich, *C. R. Chim.* **2007**, *10*, 71–78.
- [68] H. Yoon, C. J. Burrows, *J. Am. Chem. Soc.* **1988**, *110*, 4087–4089.
- [69] H. Yoon, T. R. Wagler, K. J. O'Connor, C. J. Burrows, *J. Am. Chem. Soc.* **1990**, *112*, 4568–4570.
- [70] E. F. DiMauro, M. C. Kozlowski, *Organometallics* **2002**, *21*, 1454–1461.
- [71] T. L. Siddall, N. Miyaura, J. C. Huffman, J. K. Kochi, *J. Chem. Soc. Chem. Commun.* **1983**, 1185–1186.
- [72] E. G. Samsel, K. Srinivasan, J. K. Kochi, *J. Am. Chem. Soc.* **1985**, *107*, 7606–7617.
- [73] K. Srinivasan, P. Michaud, J. K. Kochi, *J. Am. Chem. Soc.* **1986**, *108*, 2309–2320.
- [74] K. Nakajima, M. Kojima, J. Fujita, *Chem. Lett.* **1986**, 1483–1486.
- [75] V. Vincens, A. Le Borgne, N. Spassky, *Makromol. Chem. Rapid Commun.* **1989**, *10*, 623–628.
- [76] D. A. Atwood, J. A. Jegier, D. Rutherford, *J. Am. Chem. Soc.* **1995**, *117*, 6779–6780.
- [77] W. Zhang, J. L. Loebach, S. R. Wilson, E. N. Jacobsen, *J. Am. Chem. Soc.* **1990**, *112*, 2801–2803.
- [78] R. Irie, K. Noda, Y. Ito, N. Matsumoto, T. Katsuki, *Tetrahedron Lett.* **1990**, *31*, 7345–7348.
- [79] J. F. Larrow, E. N. Jacobsen, Y. Gao, Y. Hong, X. Nie, C. M. Zepp, *J. Org. Chem.* **1994**, *59*, 1939–1942.
- [80] H. Sasaki, R. Irie, T. Hamada, K. Suzuki, T. Katsuki, *Tetrahedron* **1994**, *50*, 11827–11838.
- [81] T. Hamada, T. Fukuda, H. Imanishi, T. Katsuki, *Tetrahedron* **1996**, *52*, 515–530.
- [82] Y. N. Ito, T. Katsuki, *Bull. Chem. Soc. Jpn.* **1999**, *72*, 603–619.
- [83] K. M. Ryan, C. Bousquet, D. G. Gilheany, *Tetrahedron Lett.* **1999**, *40*, 3613–3616.
- [84] H. Jacobsen, L. Cavallo, *Chem. Eur. J.* **2001**, *7*, 800–807.
- [85] J. El-Bahraoui, O. Wiest, D. Feichtinger, D. A. Plattner, *Angew. Chem.* **2001**, *113*, 2131–2134; *Angew. Chem. Int. Ed.* **2001**, *40*, 2073–2076.
- [86] L. Cavallo, H. Jacobsen, *J. Org. Chem.* **2003**, *68*, 6202–6207.
- [87] D. J. Darensbourg, R. M. Mackiewicz, J. L. Rodgers, C. C. Fang, D. R. Billodeaux, J. H. Reibenspies, *Inorg. Chem.* **2004**, *43*, 6024–6034.
- [88] L. Cavallo, H. Jacobsen, *Eur. J. Inorg. Chem.* **2003**, 892–902.
- [89] M. Bandini, P. G. Cozzi, A. Umanchi-Ronchi, *Chem. Commun.* **2002**, 919–927.
- [90] R. G. Konsler, J. Karl, E. N. Jacobsen, *J. Am. Chem. Soc.* **1998**, *120*, 10780–10781.
- [91] E. N. Jacobsen, *Acc. Chem. Res.* **2000**, *33*, 421–431.
- [92] The program package JulX was used for spin-Hamiltonian simulations and fitting the data by a full-matrix diagonalization approach; E. Bill, unpublished results.
- [93] R. Ahlrichs, M. Bär, M. Häser, H. Horn, C. Kölmel, *Chem. Phys. Lett.* **1989**, *162*, 165–169.
- [94] A. D. Becke, *Phys. Rev. A* **1988**, *38*, 3098–3100.
- [95] J. P. Perdew, *Phys. Rev. B* **1986**, *33*, 8822–8824.
- [96] K. Eichkorn, O. Treutler, H. Öhm, M. Häser, R. Ahlrichs, *Chem. Phys. Lett.* **1995**, *242*, 652–660.
- [97] K. Eichkorn, F. Weigend, O. Treutler, R. Ahlrichs, *Theor. Chem. Acc.* **1997**, *97*, 119–124.
- [98] A. Schäfer, C. Huber, R. Ahlrichs, *J. Chem. Phys.* **1994**, *100*, 5829–5835.
- [99] M. Heidemeier, T. Glaser, T. Weyhermüller, unpublished results.
- [100] S. Zolezzi, E. Spodine, A. Decinti, *Polyhedron* **2002**, *21*, 55–59.
- [101] P. Audebert, P. Capdevielle, M. Maury, *New J. Chem.* **1991**, *15*, 235–237.
- [102] J. Ferguson, *J. Chem. Phys.* **1961**, *35*, 1612–1616.
- [103] R. S. Downing, F. L. Urbach, *J. Am. Chem. Soc.* **1969**, *91*, 5977–5983.
- [104] M. M. Bhadbhade, D. Srinivas, *Inorg. Chem.* **1993**, *32*, 6122–6130.
- [105] A. R. Amundsen, J. Whelan, B. Bosnich, *J. Am. Chem. Soc.* **1977**, *99*, 6730–6739.
- [106] T. Hoshi, Y. Inomaki, M. Wada, Y. Yamada, J. Okubo, M. Kobayashi, H. Inoue, *Ber. Bunsen-Ges. Phys. Chem.* **1994**, *98*, 585–591.
- [107] S. Di Bella, I. Fragalà, I. Ledoux, T. Marks, *J. Am. Chem. Soc.* **1995**, *117*, 9481–9485.
- [108] S. Di Bella, I. Fragalà, T. Marks, M. A. Ratner, *J. Am. Chem. Soc.* **1996**, *118*, 12747–12751.
- [109] R. Klement, F. Stock, H. Elias, H. Paulus, P. Pelikán, M. Valko, M. Mazúr, *Polyhedron* **1999**, *18*, 3617–3628.

- [110] R. C. Pratt, T. D. P. Stack, *J. Am. Chem. Soc.* **2003**, *125*, 8716–8717.
- [111] T. Glaser, I. Liratzis, O. Kataeva, R. Fröhlich, M. Piacenza, S. Grimme, *Chem. Commun.* **2006**, 1024–1026.
- [112] F. Thomas, O. Jarjayes, C. Duboc, C. Philouze, E. Saint-Aman, J.-L. Pierre, *Dalton Trans.* **2004**, 2662–2669.
- [113] Y. Shiraishi, N. Saito, T. Hirai, *J. Am. Chem. Soc.* **2005**, *127*, 8304–8306.
- [114] M. B. Robin, P. Day, *Adv. Inorg. Chem. Radiochem.* **1967**, *9*, 247–422.
- [115] Y. Takano, T. Onishi, Y. Kitagawa, T. Soda, Y. Yoshioka, K. Yamaguchi, *Int. J. Quantum Chem.* **2000**, *80*, 681–691.
- [116] M. Yasui, Y. Ishikawa, N. Akiyama, T. Ishida, T. Nogami, F. Iwasaki, *Acta Crystallogr. Sect. B* **2001**, *57*, 288–295.
- [117] F. Mohri, K. Yoshizawa, T. Yamabe, T. Ishida, T. Nogami, *Mol. Eng.* **1999**, *8*, 357–373.
- [118] P. Karafiloglou, *J. Chem. Phys.* **1985**, *82*, 3728–3740.
- [119] J. Cano, E. Ruiz, S. Alvarez, M. Verdaguier, *Comments Inorg. Chem.* **1998**, *20*, 27–56.
- [120] A. Bencini, D. Gatteschi, F. Totti, D. N. Sanz, J. A. McCleverty, M. D. Ward, *J. Phys. Chem. A* **1998**, *102*, 10545–10551.
- [121] T. Glaser, B. Hedman, K. O. Hodgson, E. I. Solomon, *Acc. Chem. Res.* **2000**, *33*, 859–868.
- [122] M. I. Davis, A. M. Orville, F. Neese, J. M. Zaleski, J. D. Lipscomb, E. I. Solomon, *J. Am. Chem. Soc.* **2002**, *124*, 602–614.
- [123] F. Kanno, K. Inoue, N. Koga, H. Iwamura, *J. Am. Chem. Soc.* **1993**, *115*, 847–850.
- [124] Y. M. Shen, W. L. Duan, M. Shi, *J. Org. Chem.* **2003**, *68*, 1559–1562.
- [125] S. Bunce, R. J. Cross, L. J. Farrugia, S. Kunchandy, L. L. Meason, K. W. Muir, M. O'Donnell, R. D. Peacock, D. Stirling, S. J. Teat, *Polyhedron* **1998**, *17*, 4179–4187.
- [126] A. Böttcher, H. Elias, E.-G. Jäger, H. Langfelderova, M. Mazur, L. Müller, H. Paulus, P. Pelikan, M. Rudolph, M. Valko, *Inorg. Chem.* **1993**, *32*, 4131–4138.
- [127] D. Banti, Y. N. Belokon, W. L. Fu, E. Groaz, M. North, *Chem. Commun.* **2005**, 2707–2709.
- [128] T. R. J. Achard, L. A. Clutterbuck, M. North, *Synlett* **2005**, 1828–1847.
- [129] Y. N. Belokon, J. Fuentes, M. North, J. W. Steed, *Tetrahedron* **2004**, *60*, 3191–3204.
- [130] T. R. J. Achard, Y. N. Belokon, J. Fuentes, M. North, T. Parsons, *Tetrahedron* **2004**, *60*, 5919–5930.
- [131] Y. N. Belokon, M. North, T. D. Churkina, N. S. Ikonnikov, V. I. Maleev, *Tetrahedron* **2001**, *57*, 2491–2498.

Received: May 23, 2007

Revised: July 27, 2007

Published online: October 15, 2007